TITLE: Exosomes are vehicles for the stress-regulated secretion of histones

AUTHORS:

Birendra Singh[1§], Marcus Fredriksson Sundbom[1§], Uma Muthukrishnan[2†], Balasubramanian Natarajan[2#], Stephanie Stransky[3], André Görgens[4,5,6], Joel Z. Nordin[4], Oscar P. B. Wiklander[4], Linda Sandblad[7], Simone Sidoli[3,] Samir EL Andaloussi[4], Michael Haney[1*], and Jonathan D. Gilthorpe[2*]

[§]Contributed equally and should be considered as first authors.

*Considered as co-senior authors.

[1]Department of Diagnostics and Intervention, Umeå University, Umeå, 90 185. Sweden.

[2]Department of Medical and Translational Biology, Umeå University, Umeå 90 187, Sweden.

[3]Department of Biochemistry, Albert Einstein College of Medicine, Bronx, NY 10461, USA.

[4]Department of Laboratory Medicine, Division of Biomolecular and Cellular Medicine, Karolinska Institute, Stockholm, Sweden, 141 86 Stockholm, Sweden.

[5]Department of Cellular Therapy and Allogeneic Stem Cell Transplantation (CAST), Karolinska University Hospital Huddinge and Karolinska Comprehensive Cancer Center, Stockholm, Sweden

[6]Institute for Transfusion Medicine, University Hospital Essen, University of Duisburg-Essen, Essen, Germany

[7]Department of Chemistry, Umeå University, Umeå 90 187, Sweden.

*Authors for correspondence: michael.haney@umu.se and jonathan.gilthorpe@umu.se

Begränsad delning

ABSTRACT

Histones are conserved nuclear proteins that function in the regulation of chromatin structure and gene expression. Interestingly, extracellular histones populate biofluids from healthy individuals and when elevated may contribute to various acute and chronic diseases. It is unknown if histones are secreted via a controlled pathway, or merely released from damaged or dying cells. We analysed cell culture models under normal and stressed conditions to identify pathways of histone secretion. We report that core and linker histones localize to extracellular vehicles (EVs) and are secreted via the multivesicular body/exosome pathway. Most histone localized to the EV membrane. Upregulation of histone secretion via EVs occurred following cellular stress, accompanied by enhanced vesicle secretion and a shift towards a population of smaller EVs. Using genetic or pharmacological intervention, we found that multiple pathways affected the localization of histones to EVs. Surface histones colocalized most frequently with EVs carrying the tetraspanin CD63. Unexpectedly, EV-associated histones lacked extensive post-translational modifications compared to nuclear histones. We show for the first time that membrane-associated histones are actively secreted from intact cells via EVs/exosomes. This fundamental discovery provides support for further investigation of the biological activity of exosome-associated histones and their role in disease.

197 words

KEY WORDS: Histone, extracellular vesicle, exosome, cellular stress, post translational modification.

INTRODUCTION

Histones are basic proteins[1] abundant in the eukaryotic nucleus. The core histones (H2A, H2B, H3 and H4) associate with DNA to form nucleosomes[2, 3] and together with linker histone H1 they form chromatosomes[4]. Hence, the overwhelming bulk of investigation into the localization and function of histone proteins has focused on their roles in chromatin organization and gene regulation within the nuclear compartment. Functions for cytoplasmic and extracellular histones have also been described[5, 6]. Perhaps the best understood paradigm for histone release by activated cells is in association with modified chromatin during neutrophil extracellular trap (NET) formation, by a specific pathway of regulated cell death known as 'NETosis'[7-11]. However, our understanding of pathways for histone secretion in non-activated cells is lacking.

Elevated levels of extracellular histones are found in biofluids from critically ill patients with conditions such as acute lung injury/acute respiratory distress syndrome (ALI)/(ARDS), sepsis, trauma, severe COVID-19 infection and mediate inflammation through toll-like receptor (TLR)-4 and TLR-2 signaling[12-19]. Increased circulating histones have been implicated in poor survival as well as in organ dysfunction [13, 20-22], mechanical ventilation, secondary infection[23], thromboembolic events and acute kidney injury [13, 14, 20-24]. The toxic effects of extracellular histones can be meliorated, for example by degradation using activated protein C, or blocking using anti-histone monoclonal antibodies or C1 esterase inhibitors. These approaches have indicated therapeutic potential, with increased survival and reduced organ dysfunction [24, 25]. However, relatively low levels of circulating histones are also found in biofluids under normal physiological conditions [26-29]. This raises important question of how histones reach the extracellular environment and whether there is a regulated pathway for histone secretion, as well as whether there is a function for extracellular/circulating histones in the non-disease state.

Histones have been frequently identified as components of extracellular vesicle (EV) proteomes (Exocarta database;[30], including microvesicles/ectosomes or apoptotic vesicles (generated via outward budding of the plasma membrane), apoptotic bodies (released via membrane blebbing), amphisomes[31], and exosomes [32, 33]. Exosomes are endosome-derived vesicles [34] formed as intraluminal vesicles from inward budding within multivesicular bodies (MVBs) and released from cells upon the fusion of an MVB with the plasma membrane [35]. They carry numerous proteins [32], bioactive lipids [36] RNAs [37] and DNA [38]. Two basic

pathways for exosome biogenesis have been defined; an endosomal sorting complex required for transport (ESCRT)-dependent and an ESCRT-independent pathway requiring ceramide [39, 40]. It is unclear whether extracellular histones are associated with a particular type of EV, whether they localize to the surface or within EVs, or how they are trafficked to a secretory pathway.

The presence of histones in purified EVs has been suggested to be due to contamination with apoptotic vesicles that co-purify [32], or fusion of EVs with free histones during ultracentrifugation [31]. Another suggestion has been that histones are sorted into the lumen of EVs with exosomal DNA (exoDNA) in a nucleosome-like configuration [41] or are secreted via mitochondrial derived EVs [6]. We have previously identified histones as secretory components of injured rat brain tissue [42]. Significant progress has been made in understanding pathways of EV/exosome biogenesis using rodent brain oligodendrocyte cell lines [43-45], which contain both core and linker histones[44]. We used this as a starting point to define whether and where histones localize to EVs and to define how they are secreted.

In this study, we used the rat oligodendrocyte progenitor cell line OLN-93[46] as a model to elucidate the pathways for EV-mediated histone secretion. Using a combination of experimental strategies, we show for the first time that core and linker histones are present in MVBs and released via exosomes. Histone secretion was upregulated in response to different stress paradigms. Surprisingly, histones were associated with the EV membrane and interacted directly with membrane lipids. Both ESCRT-dependent and –independent, as well as autophagosome-lysosomal pathways, were involved in the routing of histones for secretion. Using imaging flow cytometry, we could show both H3 and H4 colocalize to the surface of tetraspanin positive EVs, predominantly a CD63 positive population. Intriguingly, secreted EV associated histones lacked post-translational modifications, distinguishing them from their nuclear counterparts.

MATERIALS AND METHODS

Cell lines and culture

All cells were maintained in a humidified incubator at 37°C/5% (v/v) CO_2. OLN-93 cells [46] or HEK293T cells (ATCC CRL-3216) were routinely cultured in high glucose Dulbecco's modified Eagle's medium (DMEM), 2 mM L-glutamine, 10% (v/v) FBS with 100 IU/ml penicillin/streptomycin. An OLN-93$^{EGFP-CD63}$ cell line (EGFP fused to the intraluminal N-terminus of human CD63) [90] was established by selection in 1 mg/ml G418 sulphate [91]. Constructs for mouse H2A type 2-C (Hist2h2ac, Uniprot Q64523) and H3.1 (Hist1h3a, P68433) were generated by RT-PCR from mouse cDNA cloned (details available on request) into a modified doxycycline-inducible lentiviral vector pCW57.1 (a gift from David Root, Addgene plasmid # 41393). 293 [HEK-293] (ATCC® CRL-1573TM) stable cell lines were generated via transduction of lentiviral particles and selection with 2.5 μg/ml puromycin (Sigma) for 4 days. Histone expression was induced by addition of 1 μg/ml doxycycline (Sigma) for 24 h.

Antibodies

Primary antibodies used were; Anti-histone H1 (clone AE-4, 05-457), anti-pan histone (clone), anti-H3-CT (07-690), anti-H2A acidic patch (07-146), anti-H2B (07-371) and anti-H4 (05-858, clone 62-141-13) purchased from Millipore. Anti-H2A (Novus NBP1-58095), Anti-H1 (orb10806, Biorbyt; 39708, Active Motif), anti-human CD63 (clone 12,435, Fitzgerald), Anti-human CD63 (Pierce MA119281) anti-rat CD63 (NBP2-68077, Novusbio), anti-CD9 (C-4, Santa Cruz; C9993 Sigma; Novus NBP2-67310), (anti-GFP (Clones 7.1 and 13.1, Roche), anti-actin, beta (A1978, Sigma), anti-acetylcholine esterase (AChE) and anti-TSG101 (ab97299 and ab83, Abcam), anti-GM130 (610823, BD Transduction), anti-HSP60 (4869, Cell Signaling) and anti-hsp70 (SPA-812, Stressgen Bioreagents). Annexin A1 (AF3770, R&D Systems). Alexa fluor conjugated secondary antibodies from Molecular Probes/Thermo Fisher Scientific were used for immunofluorescence.

Western blot

All protein concentrations were estimated using BCA Protein Assay Kit (Pierce/Thermo Fisher Scientific) and proteins were separated by SDS-PAGE on AnykD Criterion™ TGX™ precast gels (Bio-Rad) and transferred to 0.2 μm nitrocellulose membranes by using Trans-

blot Turbo (Bio-Rad) instrument. Blots were blocked and then incubated with primary and HRP-conjugated secondary antibodies (Vector Labs or Dako), followed by detection with ECL Prime Western Blot Detection (GE Healthcare). Blots were imaged in a Odyssey®CLx system /LI-COR).

EV production and isolation

Cells were seeded in T-175 tissue culture flasks coated with 50 ug/ml poly-D-lysine and grown to confluence in complete DMEM in a humidified incubator at 37°C/5% (v/v) CO_2. Cells were washed 3x with PBS and serum-free Opti-MEM media was added and incubated for 24 h. EVs were isolated from conditioned medium by sequential centrifugation [92] at 500 *x*g for 10 min, 2,000 *x*g for 20 min, 10,000 *x*g for 30 min (to remove cell debris and larger microvesicles) followed by a 0.2 µm filtration step. Large volumes of EV containing media was concentrated by using tangential cross flow ultrafiltration (100 kDa MWCO, Sartorius). EVs were collected in a refrigerated ultracentrifuge at 100,000-110,000 *x*g for 90 min (Optima XPN-100 ultracentrifuge using a SW28 or SW32Ti rotor, Beckman Coulter). EVs were subject to 2 washes in 50 mM HEPES pH 7.4 containing 150 mM NaCl with recovery at 100,000 *x*g for 90 min. EVs were used after resuspension or stored in the same buffer at -80°C after snap freezing in liquid nitrogen. The protein content, dsDNA and ssDNA content of EVs was quantified with a Qubit 3.0 fluorometer using the Qubit protein, dsDNA HS and ssDNA HS assay kits (Life Technologies/Thermo Fisher Scientific).

EVs were also produced at scale from OLN-93 cells grown in a hollow fibre bioreactor (FiberCell Systems, USA). Cells were seeded/maintained and harvested according to the manufacturer's protocol. Complete DMEM used as a reservoir feeding media. The cell compartment of bioreactor was supplemented with OptiMEM or OptiMEM+10% EV-free FBS. Harvesting of the bioreactor was performed at a regular 12 h interval and overgrowth of the cells was controlled by flushing the bioreactor, as described in the manufacturer's instructions.

OptiPrep equilibrium density gradient centrifugation

Iodixanol (OptiPrep) density gradients were used to separate 300-400 µg of EVs (based on protein content) from a 100,000 *x*g pellet fraction, according to the manufacturer's protocol. In brief, a 12-36% (w/v) OptiPrep gradient was prepared in 25 mM Hepes, 150 mM NaCl

(pH 7.4), 0.25 M sucrose, 1 mM EDTA and 10 mM Tris-HCl (pH 7.4). EVs were then placed in the bottom 36% layer of a 6-step gradient in a 13.2 ml open top polyallomer tube (331372, Beckman Coulter). A reference gradient was prepared in parallel and OptiPrep absorbance was measured at 340 nm to estimate the fraction density. Following ultracentrifugation at 100,000 *x*g for 18 h (SW41 Ti rotor), fractions were collected and washed with 25 mM HEPES, 150 mM NaCl (pH 7.4) for 4 hours at 100,000 *x*g. Pellets were resuspended in PBS or HEPES buffer. If required, fraction 4-7 were pooled and it is called $EVs^{Optiprep}$.

Immunofluorescence staining and Duolink Proximity Ligation Assay (PLA)

OLN-93 or HEK293T in Opti-MEM were grown on poly-D-lysine coated glass coverslips for 16 h under normal culturing conditions. Paraformaldehyde was added at a final concentration of 4% to fix the cells and incubated for 15 min at RT. Cells were then washed three times with PBS and then blocked in 10% FBS 0.1% Triton-X 100 for 1 h at RT. Blocking solution was removed and primary antibodies were added and incubated overnight at 4°C. The next morning the samples were washed 3 x 5 min followed by addition of fluorophore conjugated secondary antibodies. After 1 hour at RT, coverslips were again washed 3 times with PBS and then mounted with Dako Fluorescence Mounting Medium and imaged using a confocal microscope (Nikon Eclipse C1).

For PLA, permabilization, blocking and primary antibody incubation was carried out like described above. DuoLink PLA (Sigma was performed according to the manufacturer's protocol. In brief, PLA probes were incubated with the samples for 1h at 37°C in a humidity chamber, followed by 30 min ligation and 100 min amplification in the same conditions. After washing, samples were added with DAPI and briefly washed in ddH2O. Cover slips were mounted with Dako Fluorescence Mounting Medium and imaged using a confocal microscope.

Cellular stress

Cells were seeded in T-25/T-175 tissue culture flasks or coverslips coated with 50 ug/ml poly-D-lysine and grown to confluence in complete DMEM. Cells were then washed 3x with PBS and switched to serum-free conditions in Opti-MEM. For heat stress experiments, after 24 h the conditioned medium was collected (control/before) before subjecting the cells to heat stress at 42°C. After a 3 h heat shock, the cells were returned to 37°C for 4 h recovery. EV-conditioned medium was collected (heat stress sample) and replaced with fresh Opti-

MEM. Conditioned medium was again collected after a further 17 h (after sample). For other stress experiments, control samples were maintained in parallel with treated samples. LPS stress (1 µg/ml from *E. coli O111:B4*), oxidative stress (single application of 50 µM H_2O_2) or hypoxia (2% O_2, 5% CO_2, balance N_2) were performed for 24 h.)

Cell viability assays

OLN-93 cells were seeded on to coverslips or in 96-well cell culture plates (fluorescence compatible) coated with poly-D-lysine and grown to 80-90% confluency. Cells were washed 3x with PBS and switched to Opti-MEM. Following stress exposure, cells were stained with Hoechst 33342 and propidium iodide. Media was removed and PBS containing Hoechst 333421 (5 µg/ml) and propidium iodide (5 µg/ml) for 20 min at RT. Cells were washed 1x with PBS and coverslips were mounted and imaged in confocal microscope (Nikon Eclipse), or microtiter plates subjected to fluorescence cell imaging (Spark cyto, Tecan).

Apoptosis was quantified using the IncuCyte platform (Sartorius). OLN-93 cells were seeded (7000 cells/well) in 24-well plates (Corning, Cat. No.3526) coated with poly-D-lysine. Cells were incubated overnight at 37°C and 5% CO_2. Cells were washed 3x with PBS and switched to Opti-MEM. Annexin V-red and Cytox-green reagents (Sartorius) were added according to the manufacturer's recommendations. The cells were subjected to stress conditions and the cells were imaged every 2 h over a 24 h period. The number of labelled cells in each channel was quantified and analysed using the IncuCyte software.

Nanoparticle tracking analysis

Nanoparticle tracking analysis (NTA) was used to determine the size distribution and number of particles [93] using a NanoSight NS300 instrument (Malvern Instruments, UK) equipped with NTA 3.1 software. For all our recordings, a camera level of 8-9 and a detection threshold of 3-4 were used. Samples were diluted in HEPES to achieve a particle concentration of approximately $2x10^8$-$1x10^9$ particles/ml. Five 60 s videos were analysed for each sample and measurements were repeated for 3-5 replicate samples.

High resolution single EV imaging flow cytometry

EVs were analysed at a single vesicle level by high resolution imaging flow cytometry (IFCM; Amnis Cellstream, Cytek; equipped with 405, 488, 561 and 642 nm lasers) based on previously optimized settings and protocols [65, 67, 94]. Briefly, fluorescently conjugated anti-

histone and anti-tetraspanin antibodies were used to probe for respective proteins on the EV surface in pre-cleared conditioned media (CM) samples collected from HeLa cells for control and H_2O_2 treatment. For each measurement, 25 µl of CM (and unused control media) were incubated with the respective antibodies overnight at room temperature. The following antibodies were used: CD9-APC (Miltenyi Biotech, clone SN4, 130-128-037; final staining concentration 0.6 ng/µl), CD63-APC (Miltenyi Biotec, clone H5C6, 130-100-182; 0.6 ng/µL), CD81-APC (Beckman Coulter, clone JS64, A87789; 0.6 ng/µl), H3-AF488 (Invitrogen, clone 17H2L9, MA7-02023-A488; 2 ng/µL), and H4-FITC (Novus Biologicals; polyclonal, NB21-2044F; 2 ng/µL). For detergent lysis controls, samples were treated with 0.5 % NP-40 for 30 min at RT post staining. All samples were diluted 50-500-fold in PBS-HAT [95] before acquisition by using the autosampler of the Cellstream instrument with FSC turned off, SSC laser set to 40%, and all other lasers set to 100% of the maximum power. Samples and all controls were acquired for 3-5 minutes at a flow rate of 3.66 µl/minute with CellStream software version 1.2.3 and analysed with FlowJo Software version 10.8.1 (FlowJo, LLC). Fluorescence calibration and reporting of fluorescence data in molecules of equivalent soluble fluorophores (MESF) was performed as described before [65, 67]. Dulbecco's PBS pH 7.4 (Gibco) was used as instrument sheath fluid.

NaCl and lithium 3,5-diiodosalicylate treatment of EVs

NaCl and Li-diiodosalicylate were used for selective extraction of proteins from purified EV fractions (5 µg in 20 mM Tris-HCl, pH 7.5) using NaCl (250 mM-1.0 M) or Li-diiodosalicylate (5-50 mM). The final volume was adjusted to 25 µl using Tris-HCl. Samples were incubated for 12 h at 4ºC with gentle shaking. The next day, 5 µl of the sample was taken for TEM analysis and 20 µl was subjected to ultracentrifugation at 150,000 *x*g in a TLA-100 rotor and benchtop ultracentrifuge (Optima Max-XP, Beckman Coulter) for 1h at 4ºC. Supernatants and pellet fractions were analysed by SDS-PAGE and WB.

Lipid isolation and liposome preparation

Lipids from intact OLN-93 cells were extracted as described [57]. In brief, cells from 5x T-175 culture flasks containing grown to 90 % confluency, were trypsinized and collected by centrifugation. Pellets were then resuspended in 3 ml of chloroform/methanol mix (1:2) and incubated for 30 min with mixing every 5 minutes by vortexing. Chloroform (500 µL) was added together with 900 µL deionized water and samples were centrifuged at 1300 *x*g then incubated for 10 min at RT. The organic bottom phase was collected and 500 µl chloroform

and 900 µl deionized water was added, after which the sample was centrifuged again at 1300 *x*g for 10 min at RT. The organic phase was collected and dried with a gentle stream of nitrogen under constant rotation. Samples were then additionally dried using a vacuum pump for 3 h. Dried lipids were rehydrated overnight in HEPES buffer 50 mM, 150 mM NaCl pH 7.4 and sonicated briefly in a sonicating water bath. Following rehydration, the liposomes were homogenized using a 100 nm membrane Mini-Extruder (Avanti Polar Lipids). The sample was heated to 65°C and the sample then passed through a 100 nm membrane 30 times. Size distribution was confirmed by NTA, and morphology was confirmed by TEM.

Histone and liposome binding experiments

Human recombinant histones from New England Biolabs: H1 (M2501S), H2A (M2502S), H2B (M2505S), H3.1 (M2503S) and H4 (M2504S), or histones extracted from calf thymus (H3250 IIA Sigma) were used. For binding studies,10 µg of liposomes (in 50 mM HEPES buffer containing 150 mM NaCl, pH 7.4) were mixed with 1 µg histone and incubated for 1 h at RT under gentle agitation. Histones without liposomes was used as controls. Samples were loaded onto 100 kDa MWCO centrifugal filters (Millipore) and washed seven times by centrifugation with HEPES pH 7.4 containing 150 mM NaCl. Histones bound to liposomes were analysed using WB. Liposome fractionation was performed on a sucrose gradient [56]. Liposome-histone samples were loaded in the bottom in a 40% sucrose layer, with the discontinuous step gradient going up to 0% sucrose. Samples were then spun at 100,000 *x*g for 16 h at 4°C using a TLS-55 swinging-bucket rotor and benchtop ultracentrifuge (Optima Max-XP, Beckman Coulter). Fractions were collected and loaded in SDS-PAGE for WB.

DNase I and trypsin treatment of EVs

EVs (10 µg) were treated with 4 U of TURBO^{TM} DNase I (Life Technologies) in PBS with or without 0.1% (v/v) Triton X-100 in a 20 µl reaction at 37°C for 30 min. ssDNA and dsDNA were analysed by Qubit assay, and histones using WB. EVs derived from OLN-93$^{CD63\text{-}RFP}$ cells were suspended in HEPES buffer (50 mM 4-(2-hydroxyethyl)-1-piperazineethanesulfonic acid, pH 7.5) and treated for 30 min. at 37°C with Trypsin Protease, MS Grade (Pierce/Thermo Fisher Scientific) at ratios of 1:1500, 1:500 and 1:150 µg trypsin:µg protein in a total volume of 60 µl. Control EVs were incubated without trypsin. Trypsin was inhibited using 10 µM phenylmethylsulfonyl fluoride (PMSF, Roche Diagnostics) in a total volume of 1ml PBS for 10 min. on ice. EVs were washed in PBS and pelleted at 110,000 g for 1 h prior to WB.

Nuclear and cytoplasmic extract preparation and histone extraction

Cells were pelleted by centrifugation and resuspended in HEPES 10 mM (pH 7.9), 1.5 mM $MgCl_2$, 10 mM KCl, 2 mM DTT with Protease inhibitor cocktail (Roche) and incubated for 10 min on ice. Sample were then pelleted at 2000 *x*g again at 4ºC and resuspended in the same buffer, followed by homogenization with a Dounce homogenizer. After centrifugation at 10,000 *x*g for 10 min at 4ºC the supernatant was collected as the cytoplasmic extract and the pellet was resuspended in 20 mM HEPES pH 7.9, 1.5 mM $MgCl_2$, 500 mM NaCl, 25 % glycerol, 0.5 mM EDTA, 1 mM DTT and protease inhibitors and incubated for 30 min at 4ºC with continuous mixing. The mixture was then centrifuged, and supernatant collected as nuclear extract.

Acid extraction of histones followed with the addition of 0.4 M H_2SO_4 for 2 h at RT [96]. Following centrifugation, TCA was added to the supernatant at a final concentration of 20%. The mixture was incubated for 2 h at RT before centrifugation. The pellet was retrieved and washed 3x with acetone before air drying. Histones were dissolved in ddH_2O.

StrataClean pull down of proteins

Cell culture media was cleared by 500, 2000, and 10,000 *x*g sequential centrifugation steps followed by 0.2 µm filtration. StrataClean resin (Agilent) was added to the media (5 µl/ml). Thereafter, samples were placed on a roller for 15 h at 4 ºC. Finally, the resin was collected by centrifugation 5,000 *x*g for 10 min. Total protein bound resin was resuspended in 1X SDS-PAGE loading buffer containing 2 mM fresh DTT. Before loading on SDS-PAGE, samples were boiled in 95 ºC for 10 min. Protein were characterised by WB.

Pharmacological treatments of cells

Drug concentrations were selected from previously published protocols (Supplementary table S1) Cell viability was tested following treatment with a range of drug concentrations using the MTT assay. Cells were grown 96-well plates treated with in poly-D-lysine. After washing cells with PBS, drugs were applied in serum-free media (OptiMEM) in a set of 6 replicates. After 24 h of incubation, 10 µl freshly prepared MTT (Sigma; 5 mg/ml in ddH_2O) was added to each well. Cells were incubated for 3 h at 37ºC. Media was carefully aspirated and 50 µl DMSO was added to each well to dissolve formazan crystals. Absorbance at 560 nm was read in a plate reader (Biotech Synergy 2). Wells without cells were used as controls.

For analysis of secreted histones, OLN-93 cells were grown in poly-D-lysine coated T-25 flasks until 80-90% confluency. Cells were washed with PBS and 2.5 ml OptiMEM supplemented with drug or vehicle (control) were added to each well. According to the results of the MTT optimization, 10 mM 3-methyl adenine (3-MA, Sigma), 5 µM neutral sphingomyelinase inhibitor GW4869 (SelleckChem), 200 mM trehalose (Merck), 50 µM imipramine (SelleckChem), 25 µM rapamycin (SelleckChem), 100 nM Bafilomycin A1 (SelleckChem), 15 µM Dyngo (SelleckChem), 10 mM valproic acid (Sigma), 10 mM sodium butyrate (Sigma), 200 nM Trichostatin A (Sigma), 20 nM romidepsin (SelleckChem), 50 µM YF-2 (SelleckChem), 15 µM C646 (SelleckChem), 10 µM A-485 (SelleckChem) were used. After 24 h of incubation, supernatant (conditioned media) was removed from the flasks. Conditioned media (2 mL) was taken and processed at 500 *x*g /10 min, 2,000 *x*g /20 min, 10,000 *x*g /30 min (to remove cell debris and larger microvesicles) followed by protein pull down using StrataClean resin.

Histone preparation and analysis in mass spectrometry

Histones were prepared as described [96]. Briefly, histones were acid-extracted with chilled 0.2 M sulfuric acid (5:1, sulfuric acid:pellet) and incubated with constant rotation for 4 h at 4ºC, followed by precipitation with 33% trichloroacetic acid (TCA) overnight at 4ºC. The pellet was dissolved in 50 mM ammonium bicarbonate, pH 8.0, and histones were subjected to derivatization using 5 µl of propionic anhydride and 14 µl of ammonium hydroxide (all Sigma Aldrich) to balance the pH at 8.0. The mixture was incubated for 15 min and the procedure was repeated. Histones were then digested with 1 µg of sequencing grade trypsin (Promega) diluted in 50 mM ammonium bicarbonate (1:20, enzyme:sample) overnight at room temperature. Derivatization reaction was repeated to derivatize peptide N-termini. The samples were dried in a vacuum centrifuge.

Samples were resuspended in 10 µl of 0.1% TFA and loaded onto a Dionex RSLC Ultimate 300 (Thermo Scientific), coupled online with an Orbitrap Fusion Lumos (Thermo Scientific). Chromatographic separation was performed with a two-column system, consisting of a C-18 trap cartridge (300 µm ID, 5 mm length) and a picofrit analytical column (75 µm ID, 25 cm length) packed in-house with reversed-phase Repro-Sil Pur C18-AQ 3 µm resin. Peptides were separated using a 30 min gradient from 1-30% buffer B (buffer A: 0.1% formic acid, buffer B: 80% acetonitrile + 0.1% formic acid) at a flow rate of 300 nl/min. The mass

spectrometer was set to acquire spectra in a data-independent acquisition (DIA) mode. Briefly, the full MS scan was set to 300-1100 m/z in the orbitrap with a resolution of 120,000 (at 200 m/z) and an AGC target of 5x10e5. MS/MS was performed in the orbitrap with sequential isolation windows of 50 m/z with an AGC target of 2x10e5 and an HCD collision energy of 30.

Histone peptides raw files were imported into EpiProfile 2.0 software [97]. From the extracted ion chromatogram, the area under the curve was obtained and used to estimate the abundance of each peptide. To achieve the relative abundance of post-translational modifications (PTMs), the sum of all different modified forms of a histone peptide was considered as 100% and the area of the specific peptide was divided by the total area for that histone peptide in all of its modified forms. The relative ratio of two isobaric forms was estimated by averaging the ratio for each fragment ion with different mass between the two species.

Negative contrast staining and immuno--transmission electron microscopy

EVs were visualised by negative staining as described elsewhere [47]. A total of 4 µL of sample was adsorbed to glow discharged, formvar/carbon coated copper grids. Following two washes in deionized water, negative contrast staining was performed in 1.5% (w/v) uranyl acetate for 30 s and dried at RT. Immuno-TEM on EVs was performed as previously described [98] with slight modification. Samples were absorbed in copper grids and blocked by 0.1% gelatin and 1% BSA in PBS for 1 h at RT. After brief washing in PBS, grids were incubated in primary antibodies (see Antibodies section, above) diluted in PBS containing 1% BSA and incubated overnight at 4ºC. Grids were washed in PBS and incubated with 10 nm protein A-gold particles (PAG10, BBI Solutions) for 1 h at RT. Excess PAG10 were washed by using PBS. Finally, the grids were washed 5 times in water and exposed to 1.5% uranyl acetate for 30 s and dried at RT before imaging.

Immuno-TEM on cells was performed according to published methods [99]. OLN-93 cell sections were processed according to Tokuyashu method [100]. Cells were fixed in freshly prepared EM fix solution containing 2% PFA and 0.2% glutaraldehyde. Fixation was completed by using a microwave incubator (PELCO BioWave). After fixation cells were centrifuged for 5 min at 500 *x*g and the fixative solution was replaced with PBS containing 10 mM glycine to quench free aldehyde groups. Thereafter, 3x PBS washes were performed and cells were resuspended in 12% gelatin and incubated 1h at 37°C. Gelatin blocks were

resuspended in 2.3 M sucrose and kept overnight at 4°C in a rocker shaker. Blocks were mounted on the top of metal pins and snap frozen into liquid N_2. Cryo sectioning (70 nm sections) was performed in a Leica UC7 cryostat (Leica Microsystems), and sections were mounted on copper 300x300 grids. Grids containing sections were kept in PBS and incubated at 37°C for 1 h followed by incubation in 10 mM glycine. After 3x wash in PBS grids were blocked in 1% BSA+ 0.1% gelatin solution. Primary antibodies for histone H1 and CD63 were added to the grids and incubated overnight at 4°C. After 5x washes in PBS, secondary antibody-gold or protein-A gold conjugates were added to the grids. Finally, grids were washed extensively in PBS and contrast enhanced with uranyl acetate/methylcellulose (1:4%) solution. Control grids without primary antibodies were always prepared in parallel to estimate the specificity and background. Specimens were examined with a Jeol 1230 or Talos electron microscope at 80 kV and micrographs were collected with a Gatan MSC 600CW CCD camera using Digital Micrograph software.

Statistics

Statistical analyses were performed using Graph Pad Prism 5.0c (GraphPad Software, La Jolla, CA, USA) or SPSS 26 (IBM, Armonk, NY, USA). Error bars represent standard error of mean. Data was assessed for normality using Shapiro-Wilk test. Results were analysed for statistical significance by one-way or two-way analysis of variance (ANOVA) followed by the Bonferroni and Sidak`s post hoc test. Treatment effects were assessed using paired sample T-test.

RESULTS

Histone association with extracellular and intraluminal vesicles

OLN-93 cells could be grown for several days under serum-free conditions, or to a high density in a bioreactor, facilitating the isolation of EVs by sequential centrifugation [47]. When compared to whole cell lysate by western blotting (WB), significant enrichment of membrane localized tetraspanins CD9 and CD63, as well as the luminal markers tumor susceptibility gene 101 (Tsg101) and actin beta (Actb), were observed in the 100,000 *x*g pellet fraction ($EVs^{100,000\ xg}$; Fig. 1A). Lack of contamination with cellular organelles was confirmed by absence of the cis-Golgi matrix protein GM130. When the same samples were analysed for the presence of histones, robust signals for histones were observed in whole cell lysate and all core histones (H2A, H2B, H3 and H4) were identified in the EV fraction (Fig. 1A). To confirm that histones were associated with EVs, we used immunostaining together with transmission electron microscopy (immuno-TEM). We found that tetraspanin CD63 localized to the surface of EVs (Fig. 1B), as did histone H1 (Fig. 1C). Similarly, all other histones and CD9 were also detected at the surface of EVs (Fig. S1A). These results confirmed that all subtypes of histone are associated with EVs in our samples.

Secretory vesicles (exosomes) originate from MVBs. To detect and confirm the presence of histones in MVBs, we performed immuno-TEM on ultrathin sections of the cells. MVBs containing intraluminal vesicles (ILVs) were identified and MVBs/ILVs were counted according to immuno-TEM directed against CD63 (Fig. 1D) or histones (Fig. 1E). All MVBs examined contained CD63 positive ILVs (ranging from 3-50 per MVB). In total, 48.5% of all ILVs were labelled positively for CD63 (Fig. 1D). Histones positive ILVs ranged from 24.2% for H3 to 40.6% for H2B (Fig. S1B-E). These results indicated clearly that all histones can be found in association with ILVs prior to their secretion as exosomes.

$EV^{100,000\ xg}$ pellets were fractionated using a discontinuous density gradient (12-36% OptiPrep), which is a well-established method for the purification of small EVs/exosomes from other components such as larger microvesicles and apoptotic bodies [48, 49]. The fraction density was calculated based on a reference gradient (Fig. S2A). TEM was used to confirm the purity and morphology of EVs in each fraction (Fig. S2B). EVs ranging from 30-150 nm with an intact morphology localized to fractions 4-7 (Fig. S2B). WB confirmed enrichment of CD63 in fractions 3-9 (1.05-1.14 g/ml) and most abundantly in fractions 6-7 (1.09-1.11 g/ml, Fig. 1F). CD9, Tsg101, and ALG-2-interacting protein X (ALIX/PDCD6IP) showed shifted

distributions in comparison to CD63, being enriched in fractions 4-6 (Fig.1F). Annexin A1, a marker of plasma membrane-derived microvesicles, was most abundant in fraction 4 (1.06 g/ml). Flotillin-1 (membrane marker) spanned fractions 2-7, whereas extracellular acetylcholinesterase (AChE) and the NG2 chondroitin sulfate proteoglycan, which is a membrane-anchored marker of oligodendrocyte progenitors, localized to fractions 4-7. The Golgi marker GM130 was seen at low levels through fractions 3-9, but Golgin-97 was not detected (Fig.1F). Thus, we were able to resolve distinct but overlapping EV populations ranging from Annexin A1 positive microvesicles (fraction 4), through Tsg101/Alix positive EVs in fractions 4-5 and CD9/CD63 tetraspanin positive EVs in fractions 5-7. Interestingly, in OLN-93 cells all four core histones and H1 localized to fractions 5-7 and were most abundant in fraction 6, identifying them as components of EVs that co-purify with CD63, CD9, Tsg101, and Alix (Fig.1F).

To see whether histones also localized to EVs in other cell lines, we separated $EV^{100,000\ xg}$ pellets from a selection of mouse and human cells with different tissue origins on OptiPrep gradients. Histone positive populations separating in fractions 5-10 were identified for all cell lines tested (HeLa, Caco-2, NSC-34, AC-16 and A549; Fig. S3). TEM analysis confirmed the presence of EVs in histone positive fractions. Interestingly, Hela EVs resolved as two distinct histone containing populations (Fig. S3, with fraction 3-4 copurifying with Alix and Tsg101). Hence, H3 seems to localize to EVs that float over 3 different density ranges – fractions 3-4 (mainly Tsg101+, Alix+; HeLa only), fractions 5-7 (tetraspanin positive; all cell lines tested) and fractions 8-9+ (NSC-34, AC-16, A549 and OLN-93 cells under stress). These data corroborated the association of histones with purified EVs of characteristic size, floating density, biochemical and ultrastructural features.

Co-localization of histones and CD63 in intraluminal vesicles

To observe if histones and tetraspanins colocalized in MVBs we tested both CD9 and CD63 antibodies in immunofluorescence. In contrast to results obtained with immuno-TEM (Fig. 1B) and WB (Fig. 1F), the anti-CD9 antibody signal was lost following detergent permeabilization necessary for immunostaining on intact cells. Therefore, we selected anti-CD63 as a marker for colocalization in subsequent immunofluorescence experiments. Confocal microscopy revealed colocalization of non-nuclear staining for all four core histones with CD63 in cytoplasmic puncta (Fig. 2A-D). Since the degree of colocalization observed was greatest with H3/CD63 (Fig. 2C), we also tested this antibody combination in a

proximity ligation assay (Duolink PLA), which has a higher spatial resolution (within 40 nm) than standard confocal fluorescence microscopy. Duolink confirmed an association of anti-H3/CD63 antibodies in cytoplasmic puncta with the morphological appearance of MVBs (Fig. 2E). No background signal was observed in the absence of primary antibodies (Fig. 2F) confirming the specificity of the assay.

To further verify the localization of histones to CD63 positive ILVs without the need to permeabilize the plasma membrane, thus facilitating the use of additional anti-histone antibodies, we used immuno-TEM with secondary antibodies conjugated with two different sizes of gold particle. OLN-93 sections were probed with anti-histone H1(10 nm gold) and anti-CD63 (5 nm gold). Results clearly indicated the presence of both types of gold particles in MVBs (Fig. 2G). Quantification showed 36.1% and 22.7% of ILVs labelled positively for CD63 and H1, respectively. Interestingly, 17.4% ILVs labelled with both anti-CD63 and anti-H1 antibodies (Fig. 2H). We also confirmed the presence of CD63 and H1 on OptiPrep purified EVs (Fig. 2I, S4). Human Hela, and Caco-2 cells were also investigated by immuno-TEM. Cells from both lines contained MVBs containing histone positive ILVs. Furthermore, OptiPrep purified EVs showed the presence of both CD63 and H1 (Fig. S5, S6). Taken together, using a range of experimental techniques, we have shown that histones are associated with ILVs inside MVBs and on secreted EVs in different cell lines. A proportion of these ILV/EVs are positive for both histone and CD63.

Histones secretion via extracellular vesicles following cellular stress

Cellular stress is a common denominator in pathological conditions where elevated circulating histones have been observed [50] and we hypothesized that stress might enhance histone secretion. Therefore, we develop a stress paradigm whereby we harvested/changed the conditioned media on OLN-93 cells (‘Before’) and then cultured them at 42 ºC for 3h, followed by a 4 h recovery period at 37 ºC (‘Heat stress’). Media was changed again and collected after 17 h (‘After’; Fig. 3A). Proteins were pulled down from 1 ml of conditioned media using StrataClean resin. EVs were isolated by 100,000 *x*g centrifugation. Both sample types were analysed in parallel by WB (constant volume for media and constant protein for EVs). We observed strong induction of the heat shock protein Hsp70 in both conditioned media and $EVs^{100,000\,xg}$ samples in heat stress, confirming the efficacy of the treatment (Fig. 3B, C). The levels of EV markers Tsg101, CD9, and Actb were not significantly altered. Interestingly, although heat stress led to an increase in the levels of extracellular histones

after stress, both in conditioned media and in the EVs$^{100,000\ xg}$ fraction, histones were enriched in EVs after stress (Fig. 3C). These data suggest that histones accumulate in the conditioned media in response to heat stress and a proportion of these histones are EV associated.

We next wanted to see whether histone secretion is part of a common stress response. In addition to heat, OLN-93 cells were exposed to the endotoxin lipopolysaccharide (LPS), low oxygen tension (hypoxia), and oxidative stress (H_2O_2) and EVs harvested after 24 hours. Cellular viability was assessed following stresses using live/dead (PI/Hoechst 33342) staining, and apoptosis (Annexin V/Cytox) assays (Incucyte, Sartorius, Germany). In live/dead assays, a significant increase in cell death was only observed after heat stress (Fig. S7 A,B; control v heat 6.7%, 5.5-7.8%, 95% CI, p <0,0001). Similarly, significant increases in Annexin V (early apoptotic), Cytox (compromised plasma membrane) and Annexin/Cytox double positive (late apoptotic/dead) cells were also observed following heat stress but not for other stress conditions (Fig, S7C, D). Interestingly, LPS treatment led to reduced AnnexinV, Cytox and double stained cells in comparisons to controls, indicating a protective effect for LPS in these cultures (Fig. S7D). These results suggests that although cell death may contribute to extracellular histones, which may then bind to EVs, or be endocytosed and sorted into ILVs and released via exosomes, histones present in EV fractions do not correlate clearly with elevated apoptosis or cell death.

We quantified the relative levels of histones in cytoplasmic versus EVs$^{100,000\ xg}$ fractions under control and stress conditions. All stress interventions led to a decrease in the cytoplasmic pool of H2B and H3 of between 10-64% (Fig. 3D, E). In contrast, large increases in H2B and H3 were found in EVs$^{100,000\ xg}$ fractions under all stress conditions ranging from 15-95-fold (Fig. 3D, E).

To validate the results of WB, we used immunostaining followed by confocal microscopy in intact cells. In comparison to control, enhanced anti-H3 staining was observed in cytoplasmic MVB-like compartments under all stress conditions (Fig. S8A). Annexin A1-H3 colocalization appeared unchanged under stress conditions (Fig. S9) suggesting that H3 does not associate significantly with microvesicles. Duolink staining with anti-H3 and anti-CD63 confirmed an enhanced colocalization of these 2 markers under all stress conditions (Fig. S8B). Immuno-TEM was used to quantify colocalization of histones and CD63 and more precisely. Increased numbers of anti-H1 labelled (10 nm gold) and anti-CD63 labelled (5 nm

gold) particles were found in the MVBs of cells exposed to all stress conditions (Fig. 3F, S8C-G). The number of H1 positive, or H1/CD63 double positive, ILVs increased significantly under all conditions apart from oxidative stress (Fig. 3F-H). Hence, our results support the conclusion that an increase in EV associated histones is a common phenomenon following cellular stress, although interestingly quantitative differences are apparent between different stress paradigms.

DNA may associate with EVs and both double- and single-stranded (ds or ss, respectively) forms have been found inside and outside of vesicles [38, 51]. Therefore, we investigated the possible co-dependence of histones and DNA in EVs. DNA was quantified using fluorometric assays (Qubit). Levels of ssDNA were much higher than dsDNA (Fig. S10A). Removal of surface proteins using trypsin digestion resulted in a reduction of DNA. However, under conditions that removed histones (1:150 trypsin), the amount of DNA was only moderately reduced (Fig. S10A). Next, the integrity of histones in EVs was examined after removal of DNA. DNAse I treatment in the presence or absence of Triton X-100 (TX-100) did not alter the amount of histone detected by WB (Fig. S10B). Hence, histones and DNA are not dependent on one another for their association with EVs.

The above experiments were conducted in crude $EV^{100,000\ xg}$ samples. Therefore, we went further and purified EVs from all stress conditions on OptiPrep gradients. Fractions were analysed for the distribution of both ss/dsDNA (Qubit) and histone content (WB). DNA and histones increased in EVs in response to stress. Importantly, the majority of DNA localized to fractions 8-12 whereas histones were localized to the EV containing fractions 5-7 (Fig. 3I). Taken together, our findings clearly indicate that under stress conditions cells secrete significantly higher amounts of histones associated with EVs. Reduction in cytoplasmic and increase in MVB/EV associated histones suggests they are part of an active secretory process that is stress responsive. Histones do not appear to be dependent on DNA for their association with EVs.

Dynamics of extracellular vesicle size, number and histone level following stress

Changes in ESCRT family proteins are known to be associated with the size and amount of EVs [52]. To investigate if the size and quantity of EVs changed in response to stress, we analysed $EV^{100,000\ xg}$ from before, heat stress and after samples (see Fig. 3A-C) using NTA and TEM. An increase in EV secretion was seen by NTA in heat stress and after samples,

particularly after normalization for the conditioning period before = $2.6x10^7$, heat stress = $7.1x10^7$, after = $8.6x10^7$ particle/ml/h). In addition, a population of smaller diameter EVs was evident in the after sample (Fig. S11A, B). However, the sensitivity of NTA is reduced for particles of less than 50 nm so we then used TEM to estimate EV size.

TEM analysis showed a dramatic shift in the size distribution of $EVs^{100,000\ xg}$ in heat stress and after samples, with an increase in the 40-120 nm peak at the expense of the 140-200 nm peak (Fig. 4A-C). Significantly, all stress conditions led to the secretion of smaller diameter EVs in comparison to the control/before sample (Fig. 4D). We measured the diameter of EVs (n=500) from randomly selected images (n=10). For before EVs, the mean size was 87 ± 36 nm with a mode size of 100 nm (using 10 nm bins) and for post-stress conditions, it was mean size of 36-51 ± 18-36 nm with a mode size of 30 nm.

To estimate the proportion of extracellular histone associated with EVs under before, heat stress and after conditions, we quantified H3 in conditioned media (using StrataClean) and compared these with $EV^{100,000\ xg}$ pellets generated from the same samples by WB. The rate of H3 release into the media increased approximately 7-fold from before (2.3 ng/ml/h) to after heat stress (14.2 ng/ml/h; Fig. S11E). A similar relationship was seen in EVs, with H3 increasing approximately 6-fold from before (0.05 ng/µg/h) to after heat stress (0.29 ng/µg/h; Fig. S11E). Hence, the proportion of H3 associated with EVs was relatively low in comparison to total extracellular H3 but increased in response to heat stress. Our results also show that cellular stress responses seem to impinge on a common pathway resulting in a reduction in the size of EVs.

Membrane association of histones

We next aimed to understand how histones are associated with EVs. Are they localized to the outer surface of the EVs, integral to the membrane, or intraluminal? We devised a protocol combining chemical treatment, ultracentrifugation, and sonication to distinguish between histones loosely associated with the outer surface of EVs from those tightly integrated into the membrane, or in the lumen (Fig. 5A). A high concentration of NaCl is commonly used to disrupt electrostatic interactions whilst still being a non-denaturing salt [53]. The chaotropic salt lithium 3,5-diiodosalicylate can solubilize membrane associated proteins at lower concentrations, while disrupting the membrane totally at higher concentrations [54]. In addition, we used the detergent TX-100 (0.1%) to lyse EVs [55]. WB using an anti-H3 antibody was used

to monitor histone at the different stages of extraction. In parallel, TEM was used to visualize vesicle integrity. Treatment of EVs with ≥500 mM NaCl resulted in the release of H3 into the supernatant (Fig. 5B, S12A). Up to 750 mM NaCl, EV integrity was not affected (Fig. 5E, S12B). Therefore, 750 mM NaCl was used for extraction of histones loosely bound to the surface of EVs. Following this, H3 was detected in both the supernatants and pellets of crude (100,000 *x*g pellet) and OptiPrep (fractions 4-7) purified EVs (Fig. 5B). This suggests that a proportion of histones is loosely attached to the outer surface of EVs. To probe this in more detail, EV pellets recovered after 750 mM NaCl treatment were sonicated to disrupt membranes and release luminal contents. We observed a very minor H3 signal from the presumed luminal content. The remainder of H3 associated with the pellet fraction could not be extracted using NaCl (Fig. 5C). Interestingly, OptiPrep purified EVs obtained under different stress conditions showed differing amounts of surface associated H3 (extracted by 750 mM NaCl). Heat stress EVs showed the least surface associated H3, while LPS and hypoxia EVs showed the highest levels (Fig S12 C).

Histone H3 was detected in the supernatants and pellets after EVs were treated with 10-25 mM lithium 3,5-diiodosalicylate, but only in the supernatant at 50 mM (Fig. 5D). In agreement with this, TEM analysis showed that EVs remained partially intact at 25 mM lithium 3,5-diiodosalicylate, but were disrupted at 50 mM (Fig. 5D-E, S12D). This suggests that more than just electrostatic interactions contribute to histone association with the EV membrane. In agreement with this finding, TX-100 led to a portioning of H3 into both supernatant and pellet (Fig. 5D). Moreover, we observed high molecular histone species in WB after lithium 3,5-diiodosalicylate or TX-100 treatment, which have been reported for other membrane associated proteins [56]. In summary, some histones may loosely associate with integrity was disrupted at 50 mM but not the surface of EVs, likely via electrostatic interaction. However, a proportion is membrane integral, and a minor fraction may be luminal.

To further probe the potential interaction of histones with membrane lipids, we prepared liposomes from whole-cell lipid extracts of OLN-93 cells. After incubation with recombinant human histones or total histones from calf thymus, liposome-histone mixtures were washed using 100,000 kDa molecular weight cut-off ultrafiltration. Surprisingly, all histones were found to interact with liposomes and were retained by the filter even after thorough washing (Fig. 5F). To further assess lipid-histone interaction, liposome-histone mixtures were

separated on 0-40% sucrose gradients [57] and analysed by WB. The least dense fraction (1) showed the greatest signal for total histone from calf thymus. H2A, H2B, H3 and H4 were all found to partition to Fraction 1 to some degree (Fig. 5G). These experiments confirm that even recombinant histones expressed in *E.coli*, which are post-translationally unmodified, can bind directly to membrane lipids.

To provide further evidence for histone localization to the EV membrane, a range of trypsin concentrations were used to digest proteins exposed on the surface of EVs, prior to WB (Fig. 5H). Under conditions where the membrane associated proteins Tsg101 and CD9 were protected from digestion, a complete loss of the glycophosphatidylinositol (GPI)-linked outer membrane proteoglycan neural/glial antigen 2 (NG2) occurred even at the lowest trypsin:protein ratio. Interestingly, all histones were partially protected from trypsin cleavage at 1:1500-1:500, although they were removed at 1:150. Recombinant purified histones were used as control for trypsin digestion and, in contrast to EV associated histones, did not show a pattern of partial cleavage (Fig. S13) Since all anti-histone antibodies tested were directed against C-terminal epitopes (see Methods) we wished to examine whether N-terminal of C-terminal regions were equally prone to cleavage when at the surface of EVs. Human embryonic kidney 293 (HEK293) cell lines stably expressing histone H2A or H3 with an HA at the N- and a 6xHis tag at the C-terminus were generated (Fig. 5I). EVs from these two cell lines were purified and treated with trypsin as above. Reactivity towards the N-terminal HA-tag was lost with an increasing trypsin:protein ratio, whereas the C-terminal 6xHis antibody recognized one or more truncated species (Fig. 5J-K). These results confirm that histones are membrane associated proteins in EVs and that their conformations seem to differ from soluble recombinant histones.

Origin of extracellular vesicle associated histones

Histones could localize to EVs via several different pathways: i) Sorting of soluble cytoplasmic histones into MVBs via ESCRT-dependent or -independent pathways, thereby partitioning to the luminal EV compartment. ii) Acquisition of histones to the outer surface of EVs via the amphisome pathway, following fusion of autophagosomes to endosomes. iii) Endocytosis of EV or non-EV derived histones and their subsequent sorting into ILVs, where they would also localize to the outer surface of EVs. To investigate these 3 possibilities, we used both siRNA-mediated knockdown and chemical modulators (drugs) of these pathways. Drug concentrations were determined according to published observations (Table S1). We

next validated suitable concentrations that did not impact significantly on cell morphology and viability (Fig. S14). We first targeted the ESCRT-dependent and ceramide pathways of EV biogenesis using siRNAs. Efficient knockdown of the ESCRT components *Alix* or *Tsg101* led to a reduction in histone secretion (Fig. 6A). Annexin A1 was expressed at a low level in OLN-93 cells (Fig. S9) and EVs (Fig. 1F) and did not change dramatically following siRNA treatments (Fig. 6A), indicating that the microvesicle pathway was unable to compensate for exosome biogenesis/secretion. On the other hand, knockdown of the ceramide pathway using an siRNA directed against *neutral sphingomyelinase* (*Smpd2/nSMNase2*) showed only a slight decrease in H3 secretion, which was not significant. However, due to the lack of an antibody recognizing Smpd2 in WB, we could not confirm the efficiency of Smpd2 knockdown. Hence, we used the nSMNase2 inhibitor GW4869 to block ceramide production [58, 59]. Treatment of OLN-93 cells with 5 µM GW4869 completely blocked histone secretion (Fig. 6B) and indicated that the ceramide pathway is involved in translocation of histones to ILVs.

Based on the proteomic analysis of EVs and the non-vesicular secretome, it has been proposed that EV-associated histones may originate from the nucleus and be secreted via an autophagy-dependent amphisomal pathway [31]. To investigate the role of autophagy in histone secretion, we treated OLN-93 cells with the autophagy inhibitor 3-methyadenine (3-MA), which blocks phagophore formation. 3-MA treatment increased histone secretion (Fig. 6B) and a significant increase in histone localization to ILVs (Fig. 6C). On the other hand, inducers of mTOR-independent autophagy (trehalose and imipramine) showed a significant decrease in histone secretion (Fig. 6B). The mTOR-dependent inhibitor rapamycin showed a decrease in H3 secretion that was not significant. We used Bafilomycin A1 (Baf) to block the vacuolar H+-ATPase (V-ATPase) and thereby the fusion of autophagosomes and late endosomes to lysosomes [60]. Like 3-MA, Baf treatment also increased histone secretion (Fig. 6B) and histone localization to ILVs (Fig. 6C). We used the dynamin inhibitor Hydroxy Dynasore (Dyngo-4a) to investigate the requirement for clathrin-dependent endocytosis in histone secretion [61]. Dyngo treatment downregulated histones in EVs (Fig. 6B), indicating that endocytic activity may be important for histone secretion. These results indicated that blocking active endocytosis and ceramide dependent pathways inhibit histone secretion. However, inhibition of autophagosome formation and lysosomal degradation promote the partitioning of histones to ILV/MVBs (Fig. 6C) and their secretion via EVs.

Histone translocation to, and function in, the nucleus is modulated by post-translational modifications (PTMs), such as acetylation and methylation [62, 63]. Histone acetyl transferases (HATs) modify histones on Lys (L) and Arg (K) residues, thereby reducing the net charge of the protein. Hence, we postulated that acetylation status may be important for the localization to and charge dependent interaction of histones with EV membranes. Histone acetylation is counteracted by the activity of deacetylases (HDACs). To determine if acetylation status was important for histone secretion, we used drugs to either inhibit or activate HDACs or HATs. Treatment with the pan HDAC inhibitor Trichostatin A did not result in a significant reduction of histone secretion. However, both valproic acid and sodium butyrate (HDAC1 selective) reduced histone secretion (Fig. 6B). Treatment with the broad-spectrum HAT activator YF-2 showed increased histone secretion, whilst the effect of Romidepsin (HDAC1 and 2 selective) was non-significant. In contrast, the p300/CBP selective HAT inhibitors C646 and A-485 both resulted in reduced histone secretion. Hence, interfering with histone acetylation seems to lead to more secretion via EVs.

Surface association of extracellular vesicle histones and their modifications

During the multiple centrifugation and washing steps used in $EV^{100,000\ xg}$ and OptiPrep purification, a significant amount of EV associated surface proteins may be lost from the EV corona [64]. Therefore, to confirm that histones are EV surface associated proteins, we used imaging flow cytometry (IFCM) to characterize histone positive EVs in conditioned media without purification [65-67]. We identified fluorescently labelled anti-human H3 and H4 antibodies with good signal and low noise (Fig. S15A) and combined these with previously characterized anti-human tetraspanin antibodies (CD9, CD63 and CD81), to analyse EVs in the conditioned media of HeLa cell cultures, either under control conditions, or following acute exposure to H_2O_2 (Fig. 7A, S15A).

Time course measurements over a 24 h period revealed that the mean fluorescence intensity (MFI) of anti-H3 and -H4 labelling was already maximal by 2 h and remained constant out to 24 h (Fig. S15B). In contrast the MFI of anti-tetraspanin labelling increased from 2-24 h, suggesting that H3/H4 localize to EVs but that the total amount of antibody accessible histone remains constant over time. Interestingly, H3 and H4 showed different kinetics. Under control conditions, H3 positive EVs showed a gradual increase, with the highest concentration at 24 h. In H_2O_2 treated cultures, H3 positive EVs accumulated faster, with highest concentrations measured at 4 h, followed by a gradual decrease (Fig. 7B). Thus, H_2O_2

treatment appeared to promote the release of H3 positive EVs. The different kinetics of stress responsive compared to control EVs seen using IFCM may be due to a lower level of antibody accessible H3 on the EV surface. In contrast, H4 positive EVs were detected in control and H_2O_2 treated cells at similar levels up to the 8 h timepoint, and their concentration increases markedly at 24 h in the H_2O_2 treated cultures (Fig. 7B). This indicates a difference in the kinetics and/or accessibility of antibodies to H3 or H4 on EVs.

To further characterize H3 and H4 positive EVs, we performed double labelling to assess co-occurrence of H3 or H4 together with CD9, CD63, or CD81, on the same EV. About 50-60% of total fluorescence events were found to be double positive for both H3 and CD9 or CD63, while only about one third were double positive for H3 and CD81 (Fig.7C and Fig. S15C). Similarly, H4 was detected more on CD63 positive (~60%) and CD9 positive (~45%) EVs than on CD81 positive EVs (~35%; Fig. 7 D and S15C).

Since the nuclear fuctions of histones are highly dependent on post translational modifications (PTMs), we sought to characterize the extent and pattern of PTMs on EV associated histones. We extracted histones from EVs derived from control cells and those exposed to either LPS or hypoxia, as well as the nuclear fractions from the same cells (Fig. S16) and analysed histones using nano-liquid chromatography coupled to high resolution mass spectrometry. Interestingly, common PTMs including acetylation, methylation and phosphorylation were significantly reduced in EV-derived compared to nuclear histones (Fig. 7E). For example, in control EVs single H3K9Ac and H3K14Ac marks were significantly lower in comparison to the nuclear fraction. More complex modifications, such as trimethylation (Me3) of lysine residues in H3 (Fig. 7E, F) were also less abundant in EVs. Hence, histones lacking common modifications were more enriched in EVs, as well as selected mono- or dimethylations (e.g. H3K79me2; Fig. 7F). Phosphorylation on histone H3 (H3S10ph; Fig. 7F), was also more abundant in EVs, particularly following LPS treatment, indicating that a proportion of EV-associated histones may originate from mitotic chromatin (Fig. 7F). In support of our results with HDAC inhibition or HAT activation, enrichment of unmodified histones in EVs is a novel finding.

DISCUSSION

We have demonstrated that histones are a membrane associated cargo actively secreted via the MVB/exosome pathway. Despite the consistent identification of histones as abundant components of cell secretomes [30, 68], it is controversial whether extracellular histones are associated non-specifically with EVs [32, 33] and represent a component of the 'crapome' [69]. We have addressed this longstanding problem using a range of experimental approaches and shown that: i) Histones are present extracellularly in association with highly purified EVs, and intracellularly within MVBs. ii) Histones colocalize on the surface of tetraspanin positive EVs (CD63>CD9>CD81). iii) Histone secretion increases significantly in response to cellular stress. iv) Histone secretion can be blocked by interference with ESCRT-dependent, independent, or ceramide pathways of EV biogenesis and is affected by modulation of autophagy or lysosome maturation. v) EV-associated histones are distinct in their relative lack of PTMs compared to nuclear histones.

There is a long-standing debate as to whether extracellular histones are present in EVs/exosomes or associated with another type of vesicle/particle and the specific association of histones with EVs has been overlooked. An overarching view has been that if histones are present in EVs, they are a luminal cargo in a DNA-associated nucleosomal conformation [41]. More recently, it was proposed that histones are secreted as a dsDNA complex and can be separated from EVs in the non-vesicular fraction [31]. The abundance of DNA we have identified in the non-vesicular fraction of OLN-93 EVs agrees with previous findings [51]. However, our results clearly indicate that EV associated histones, but not DNA, increase significantly and consistently under different stress conditions. We did not find any evidence for an interdependence of histones and DNA in EVs.

Do histones bind to the outer membrane of EVs? In *Drosophila*, H2A and H2B are associated intracellularly with lipid drops [70], which function as a sink to supply histones for cell division and as antimicrobial effectors during bacterial infection [71, 72]. Lipid drop binding is mediated by the protein chaperone Jabba[72, 73] and although histone-lipid drop association is conserved in mammals [71], a functional homologue for Jabba has not been identified.
H1 is known to bind to synthetic liposomes and lipids of the plasma membrane [74, 75]. We have been able to show that histones can bind to purified lipids and further identified both a strong and a weaker interaction with either surface membrane proteins, or lipids and EV-histone interaction is not easily disrupted by ionic interference. In agreement with proteomic analysis

of EV membrane proteins [76], we found only a small fraction of EV-associated H3 resides within the luminal fraction and conclude that only a small fraction of H3 is found luminally.

Upregulation of histone secretion was a common response to cellular stress. However, interesting differences were observed in the kinetics, amount and density of histone positive EV fractions. Early upregulation of EV histones was observed following heat stress, together with a smaller EV size. In contrast, the levels of cytoplasmic histones were reduced but within MVBs, histones increased, suggesting that stress induces the sequestration and secretion of cytoplasmically localized histones. LPS challenge has also been shown to lead to an upregulation of EV-associated histones in mouse bone marrow-derived macrophages, which was proposed to be due to migration of nuclear histones to the cytoplasm [77]. Whatever the source of cytoplasmically localized histones, accumulation can activate signalling pathways that may lead to apoptosis [19, 78]. Hence, cells may sequester and secrete histones as part of a stress-associated survival mechanism, whereby vesicles are released continually but histones are loaded into them in a regulated manner. This may also underlie the observation that histones are routed to MVB/EVs via multiple pathways.

In clinical contexts, circulating extracellular histones have been found in various pathological [19, 79, 80] as well as non-pathological [81] states. Our findings support the idea that at least some of these circulating histones could be EV associated. However, it is unknown whether EV associated histones have a different function compared to other types of extracellular histones identified in sepsis, trauma, or cell death [19, 23]. EVs might represent a mechanism by which excess histones can be distributed to other cells [82, 83]. Alternatively, histones may populate the secretory and endosomal pathways and function as innate immune factors to rapidly respond to pathogenic stimuli, whilst buffering the detrimental effects of their highly cationic sequences. Though our findings do not address these questions, they do highlight the importance of accurate characterization of both the nature and the origin of extracellular histone/DNA complexes since they may have different biological functions as well as pathological effects.

We found that both ESCRT-dependent and ESCRT-independent pathways of EV biogenesis were important for histone secretion. MVBs are a key node in the regulation of secretory turnover, balancing degradation (via late endosome/lysosome fusion) with recycling (via fusion to the plasma membrane) [84]. In addition, we found that modulation of autophagy and

lysosome maturation significantly affected the secretion of histones. Inhibition of phagophore formation (3-MA treatment) led to a strong upregulation of H3 in EVs. Activation of autophagy (trehalose, impiramine) had an opposing effect. Furthermore, inhibition of lysosomal degradation (Baf) increased H3 secretion. Histones lack a signal sequence and thus sorting into MVBs/ILVs should occur via a non-canonical pathway. Recent findings have begun to define pathways by which cytoplasmic histones are targeted to lysosomes for Lamp 2A-mediated degradation [85, 86]. However, it is not known how cells may regulate these processes under various physiological conditions, including stress.

PTMs are known to regulate the localization of histones to [87] and within [88] the nucleus. The most studied PTMs are acetylation and methylation that are involved in the regulation of gene expression [89] and are primarily regulated via HAT and HDAC enzymes. HAT activation via YF-2 increased histone secretion, whereas HAT inhibition showed the opposite effect. Inhibition of HDAC activity also led to significant decreases in EV-associated H3. Hence, we could not easily determine how modulation of PTM status related to histone secretion. Therefore, we determined the extent of histone PTMs to understand how they might localize to EVs. The most striking finding was that EV associated histones are relatively unmodified. Marks such as H3K4me3 and H3K9me3 were almost completely depleted in EVs. These two PTMs are perhaps the most well characterized occurrences of trimethylation and define active gene expression and constitutive heterochromatin, respectively. These findings highlight that it is not just histones from open or closed chromatin that translocate to EVs; we observed a general loss of modifications that are known to have critical regulatory role in the nucleus.

In conclusion, our results show clearly that histone proteins are secreted specifically via the MVB/exosome pathway. Secretion is regulated by cellular stress responses, leading to an upregulation of histones associated with a population of smaller sized EVs. Unexpectedly, secreted histones lack many of the of PTMs of their nuclear counterparts. Understanding how histones are routed to and and sorted in to MVB for secretion, how they bind to membranes, as well as their functional significance are the next steps.

DATA AVAILABILITY

Mass spectrometry raw data availability. All raw mass spectrometry data files from this study have been submitted to the Chorus repository (https://chorusproject.org/pages/index.html) under project number 1847.

ACKNOWLEDGEMENTS

We are most grateful to colleagues who have contributed time and materials and thank Prof. C. Richter-Landsberg (Department of Biology, University of Oldenburg, Germany) for providing OLN-93 cells and Dr. R. Lodge (Department of Medicine, Laval University, Canada) for the pEGFP-C2 CD63-GFP. Hanna Levén May and Iwan Jones provided HA-Flag constructs, Sophie Rome, Giulia Corso and Mattias Hällbrink provided valuable technical advice, and Fazal Oozeer and Adrian Pini contributed with early insights into extracellular histones. Fransesca Aguilo supplied us with AChE and HDAC1 antibodies to verify nuclear/cytoplasmic extracts. For technical assistance and instrument access we acknowledge Biochemical Imaging Center at Umeå University and the National Microscopy Infrastructure, NMI (VR-RF 2019-00217) for microscopy support, and Umeå Centre for Electron Microscopy (UCEM) in association with the NMI, VR-RFI2019-00217 and VR-2018-06478.

The study was supported by Umeå University, including the Foundation for Medical Research (Insamlingsstiftelsen), Stiftelsen Forskningsfonden För Klinisk Neurovetenskap Vid Norrlands Universitetsskjukhus, Västerbotten County Council/Region Västerbotten, Kempe Foundations, Stratneuro initiative and Neurofonden.

DECLARATION OF INTEREST STATEMENT

SELA is a founder of, and consultant for, Evox Therapeutics. SELA, JN and OW are shareholders in Evox Therapeutics. The remaining authors declare no competing interests. All authors declare no conflict of interest.

REFERENCES

1. Kossel, A. Ueber einen peptonartigen Bestandtheil des Zellkerns. (1884).
2. Kornberg, R.D. Chromatin structure: a repeating unit of histones and DNA. *Science* **184**, 868-871 (1974).
3. Luger, K., Mäder, A.W., Richmond, R.K., Sargent, D.F. & Richmond, T.J. Crystal structure of the nucleosome core particle at 2.8 A resolution. *Nature* **389**, 251-260 (1997).
4. Simpson, R.T. Structure of the chromatosome, a chromatin particle containing 160 base pairs of DNA and all the histones. *Biochemistry* **17**, 5524-5531 (1978).
5. Parseghian, M.H. & Luhrs, K.A. Beyond the walls of the nucleus: the role of histones in cellular signaling and innate immunity. *Biochem Cell Biol* **84**, 589-604 (2006).
6. Singh, A., Verma, S., Modak, S.B., Chaturvedi, M.M. & Purohit, J.S. Extra-nuclear histones: origin, significance and perspectives. *Mol Cell Biochem* **477**, 507-524 (2022).
7. Brinkmann, V. *et al.* Neutrophil extracellular traps kill bacteria. *Science* **303**, 1532-1535 (2004).
8. Hiemstra, P.S. *et al.* Antimicrobial proteins of murine macrophages. *Infect Immun* **61**, 3038-3046 (1993).
9. Hirsch, J.G. Bactericidal action of histone. *J Exp Med* **108**, 925-944 (1958).
10. Miller, B.F., Abrams, R., Dorfman, A. & Klein, M. ANTIBACTERIAL PROPERTIES OF PROTAMINE AND HISTONE. *Science* **96**, 428-430 (1942).
11. Wiesner, J. & Vilcinskas, A. Antimicrobial peptides: the ancient arm of the human immune system. *Virulence* **1**, 440-464 (2010).
12. Abrams, S.T. *et al.* Circulating histones are mediators of trauma-associated lung injury. *Am J Respir Crit Care Med* **187**, 160-169 (2013).
13. Cheng, Z. *et al.* Circulating Histones Are Major Mediators of Multiple Organ Dysfunction Syndrome in Acute Critical Illnesses. *Crit Care Med* **47**, e677-e684 (2019).
14. Huckriede, J. *et al.* Histone H3 Cleavage in Severe COVID-19 ICU Patients. *Front Cell Infect Microbiol* **11**, 694186 (2021).
15. Karki, P., Birukov, K.G. & Birukova, A.A. Extracellular histones in lung dysfunction: a new biomarker and therapeutic target? *Pulm Circ* **10**, 2045894020965357 (2020).
16. Kutcher, M.E. *et al.* Extracellular histone release in response to traumatic injury: implications for a compensatory role of activated protein C. *J Trauma Acute Care Surg* **73**, 1389-1394 (2012).
17. Lv, X. *et al.* Extracellular histones are clinically relevant mediators in the pathogenesis of acute respiratory distress syndrome. *Respir Res* **18**, 165 (2017).
18. Silk, E., Zhao, H., Weng, H. & Ma, D. The role of extracellular histone in organ injury. *Cell Death Dis* **8**, e2812 (2017).
19. Xu, J., Zhang, X., Monestier, M., Esmon, N.L. & Esmon, C.T. Extracellular histones are mediators of death through TLR2 and TLR4 in mouse fatal liver injury. *J Immunol* **187**, 2626-2631 (2011).
20. Kawai, C. *et al.* Circulating Extracellular Histones Are Clinically Relevant Mediators of Multiple Organ Injury. *Am J Pathol* **186**, 829-843 (2016).
21. Ekaney, M.L. *et al.* Impact of plasma histones in human sepsis and their contribution to cellular injury and inflammation. *Crit Care* **18**, 543 (2014).
22. Yokoyama, Y. *et al.* Circulating histone H3 levels in septic patients are associated with coagulopathy, multiple organ failure, and death: a single-center observational study. *Thromb J* **17**, 1 (2019).

23. Xu, J. *et al.* Extracellular histones are major mediators of death in sepsis. *Nat Med* **15**, 1318-1321 (2009).
24. Li, Y. *et al.* Circulating Histones in Sepsis: Potential Outcome Predictors and Therapeutic Targets. *Front Immunol* **12**, 650184 (2021).
25. Wygrecka, M. *et al.* Antihistone Properties of C1 Esterase Inhibitor Protect against Lung Injury. *Am J Respir Crit Care Med* **196**, 186-199 (2017).
26. Goldfinch, G.M. *et al.* The proteome of gastric lymph in normal and nematode infected sheep. *Proteomics* **8**, 1909-1918 (2008).
27. Mittal, A. *et al.* The proteome of rodent mesenteric lymph. *Am J Physiol Gastrointest Liver Physiol* **295**, G895-903 (2008).
28. Omenn, G.S. *et al.* Overview of the HUPO Plasma Proteome Project: results from the pilot phase with 35 collaborating laboratories and multiple analytical groups, generating a core dataset of 3020 proteins and a publicly-available database. *Proteomics* **5**, 3226-3245 (2005).
29. Waga, S., Tan, E.M. & Rubin, R.L. Identification and isolation of soluble histones from bovine milk and serum. *Biochem J* **244**, 675-682 (1987).
30. Mathivanan, S. & Simpson, R.J. ExoCarta: A compendium of exosomal proteins and RNA. *Proteomics* **9**, 4997-5000 (2009).
31. Jeppesen, D.K. *et al.* Reassessment of Exosome Composition. *Cell* **177**, 428-445.e418 (2019).
32. Théry, C. *et al.* Proteomic analysis of dendritic cell-derived exosomes: a secreted subcellular compartment distinct from apoptotic vesicles. *J Immunol* **166**, 7309-7318 (2001).
33. Turiák, L. *et al.* Proteomic characterization of thymocyte-derived microvesicles and apoptotic bodies in BALB/c mice. *J Proteomics* **74**, 2025-2033 (2011).
34. Pan, B.T., Teng, K., Wu, C., Adam, M. & Johnstone, R.M. Electron microscopic evidence for externalization of the transferrin receptor in vesicular form in sheep reticulocytes. *J Cell Biol* **101**, 942-948 (1985).
35. Johnstone, R.M., Adam, M., Hammond, J.R., Orr, L. & Turbide, C. Vesicle formation during reticulocyte maturation. Association of plasma membrane activities with released vesicles (exosomes). *J Biol Chem* **262**, 9412-9420 (1987).
36. Laulagnier, K. *et al.* Mast cell- and dendritic cell-derived exosomes display a specific lipid composition and an unusual membrane organization. *Biochem J* **380**, 161-171 (2004).
37. Valadi, H. *et al.* Exosome-mediated transfer of mRNAs and microRNAs is a novel mechanism of genetic exchange between cells. *Nat Cell Biol* **9**, 654-659 (2007).
38. Thakur, B.K. *et al.* Double-stranded DNA in exosomes: a novel biomarker in cancer detection. *Cell Res* **24**, 766-769 (2014).
39. Simons, M. & Raposo, G. Exosomes--vesicular carriers for intercellular communication. *Curr Opin Cell Biol* **21**, 575-581 (2009).
40. Kim, Y.S. *et al.* The potential theragnostic (diagnostic+therapeutic) application of exosomes in diverse biomedical fields. *Korean J Physiol Pharmacol* **22**, 113-125 (2018).
41. Colombo, M., Raposo, G. & Théry, C. Biogenesis, secretion, and intercellular interactions of exosomes and other extracellular vesicles. *Annu Rev Cell Dev Biol* **30**, 255-289 (2014).
42. Gilthorpe, J.D. *et al.* Extracellular histone H1 is neurotoxic and drives a pro-inflammatory response in microglia. *F1000Res* **2**, 148 (2013).
43. Hsu, C. *et al.* Regulation of exosome secretion by Rab35 and its GTPase-activating proteins TBC1D10A-C. *J Cell Biol* **189**, 223-232 (2010).

44. Krämer-Albers, E.M. *et al.* Oligodendrocytes secrete exosomes containing major myelin and stress-protective proteins: Trophic support for axons? *Proteomics Clin Appl* **1**, 1446-1461 (2007).
45. Trajkovic, K. *et al.* Ceramide triggers budding of exosome vesicles into multivesicular endosomes. *Science* **319**, 1244-1247 (2008).
46. Richter-Landsberg, C. & Heinrich, M. OLN-93: a new permanent oligodendroglia cell line derived from primary rat brain glial cultures. *J Neurosci Res* **45**, 161-173 (1996).
47. Hedlund, M. *et al.* Human placenta expresses and secretes NKG2D ligands via exosomes that down-modulate the cognate receptor expression: evidence for immunosuppressive function. *J Immunol* **183**, 340-351 (2009).
48. Cantin, R., Diou, J., Bélanger, D., Tremblay, A.M. & Gilbert, C. Discrimination between exosomes and HIV-1: purification of both vesicles from cell-free supernatants. *J Immunol Methods* **338**, 21-30 (2008).
49. Graner, M.W. *et al.* Proteomic and immunologic analyses of brain tumor exosomes. *Faseb j* **23**, 1541-1557 (2009).
50. Chen, R., Kang, R., Fan, X.G. & Tang, D. Release and activity of histone in diseases. *Cell Death Dis* **5**, e1370 (2014).
51. Balaj, L. *et al.* Tumour microvesicles contain retrotransposon elements and amplified oncogene sequences. *Nat Commun* **2**, 180 (2011).
52. Colombo, M. *et al.* Analysis of ESCRT functions in exosome biogenesis, composition and secretion highlights the heterogeneity of extracellular vesicles. *J Cell Sci* **126**, 5553-5565 (2013).
53. Perez-Jimenez, R., Godoy-Ruiz, R., Ibarra-Molero, B. & Sanchez-Ruiz, J.M. The efficiency of different salts to screen charge interactions in proteins: a Hofmeister effect? *Biophys J* **86**, 2414-2429 (2004).
54. Riendeau, D., Lemaire, J., Maestracci, D. & Lessard, L. Selective release of inner core proteins from intestinal microvillus membrane by lithium diiodosalicylate. *Mol Cell Biochem* **71**, 45-52 (1986).
55. Osteikoetxea, X. *et al.* Differential detergent sensitivity of extracellular vesicle subpopulations. *Org Biomol Chem* **13**, 9775-9782 (2015).
56. Rath, A., Glibowicka, M., Nadeau, V.G., Chen, G. & Deber, C.M. Detergent binding explains anomalous SDS-PAGE migration of membrane proteins. *Proc Natl Acad Sci U S A* **106**, 1760-1765 (2009).
57. Bittame, A. *et al.* Lipid Extraction from HeLa Cells, Quantification of Lipids, Formation of Large Unilamellar Vesicles (LUVs) by Extrusion and in vitro Protein-lipid Binding Assays, Analysis of the Incubation Product by Transmission Electron Microscopy (TEM) and by Flotation across a Discontinuous Sucrose Gradient. *Bio-Protocol* **6** (2016).
58. Essandoh, K. *et al.* Blockade of exosome generation with GW4869 dampens the sepsis-induced inflammation and cardiac dysfunction. *Biochim Biophys Acta* **1852**, 2362-2371 (2015).
59. Yao, Y. *et al.* Blockade of Exosome Release Suppresses Atrial Fibrillation by Alleviating Atrial Fibrosis in Canines With Prolonged Atrial Pacing. *Front Cardiovasc Med* **8**, 699175 (2021).
60. Mauvezin, C. & Neufeld, T.P. Bafilomycin A1 disrupts autophagic flux by inhibiting both V-ATPase-dependent acidification and Ca-P60A/SERCA-dependent autophagosome-lysosome fusion. *Autophagy* **11**, 1437-1438 (2015).
61. McCluskey, A. *et al.* Building a better dynasore: the dyngo compounds potently inhibit dynamin and endocytosis. *Traffic* **14**, 1272-1289 (2013).

62. Bártová, E., Krejcí, J., Harnicarová, A., Galiová, G. & Kozubek, S. Histone modifications and nuclear architecture: a review. *J Histochem Cytochem* **56**, 711-721 (2008).
63. Campos, E.I. *et al.* The program for processing newly synthesized histones H3.1 and H4. *Nat Struct Mol Biol* **17**, 1343-1351 (2010).
64. Wolf, M. *et al.* A functional corona around extracellular vesicles enhances angiogenesis, skin regeneration and immunomodulation. *J Extracell Vesicles* **11**, e12207 (2022).
65. Tertel, T. *et al.* High-Resolution Imaging Flow Cytometry Reveals Impact of Incubation Temperature on Labeling of Extracellular Vesicles with Antibodies. *Cytometry A* **97**, 602-609 (2020).
66. Ricklefs, F.L. *et al.* Imaging flow cytometry facilitates multiparametric characterization of extracellular vesicles in malignant brain tumours. *J Extracell Vesicles* **8**, 1588555 (2019).
67. Gorgens, A. *et al.* Optimisation of imaging flow cytometry for the analysis of single extracellular vesicles by using fluorescence-tagged vesicles as biological reference material. *J Extracell Vesicles* **8**, 1587567 (2019).
68. Lazaro-Ibanez, E. *et al.* DNA analysis of low- and high-density fractions defines heterogeneous subpopulations of small extracellular vesicles based on their DNA cargo and topology. *J Extracell Vesicles* **8**, 1656993 (2019).
69. Mellacheruvu, D. *et al.* The CRAPome: a contaminant repository for affinity purification-mass spectrometry data. *Nat Methods* **10**, 730-736 (2013).
70. Cermelli, S., Guo, Y., Gross, S.P. & Welte, M.A. The lipid-droplet proteome reveals that droplets are a protein-storage depot. *Curr Biol* **16**, 1783-1795 (2006).
71. Anand, P. *et al.* A novel role for lipid droplets in the organismal antibacterial response. *Elife* **1**, e00003 (2012).
72. Li, Z. *et al.* Lipid droplets control the maternal histone supply of Drosophila embryos. *Curr Biol* **22**, 2104-2113 (2012).
73. Stephenson, R.A. *et al.* Sequestration to lipid droplets promotes histone availability by preventing turnover of excess histones. *Development* **148** (2021).
74. Zhao, H., Bose, S., Tuominen, E.K. & Kinnunen, P.K. Interactions of histone H1 with phospholipids and comparison of its binding to giant liposomes and human leukemic T cells. *Biochemistry* **43**, 10192-10202 (2004).
75. Lete, M.G. *et al.* Histones cause aggregation and fusion of lipid vesicles containing phosphatidylinositol-4-phosphate. *Biophys J* **108**, 863-871 (2015).
76. Cvjetkovic, A. *et al.* Detailed Analysis of Protein Topology of Extracellular Vesicles-Evidence of Unconventional Membrane Protein Orientation. *Sci Rep* **6**, 36338 (2016).
77. Nair, R.R. *et al.* LPS-Challenged Macrophages Release Microvesicles Coated With Histones. *Front Immunol* **9**, 1463 (2018).
78. Ibañez-Cabellos, J.S. *et al.* Extracellular histones activate autophagy and apoptosis via mTOR signaling in human endothelial cells. *Biochim Biophys Acta Mol Basis Dis* **1864**, 3234-3246 (2018).
79. Gould, T.J., Lysov, Z. & Liaw, P.C. Extracellular DNA and histones: double-edged swords in immunothrombosis. *J Thromb Haemost* **13 Suppl 1**, S82-91 (2015).
80. Kim, J.E., Lee, N., Gu, J.Y., Yoo, H.J. & Kim, H.K. Circulating levels of DNA-histone complex and dsDNA are independent prognostic factors of disseminated intravascular coagulation. *Thromb Res* **135**, 1064-1069 (2015).
81. Holdenrieder, S. *et al.* Circulating nucleosomes in serum. *Ann N Y Acad Sci* **945**, 93-102 (2001).

82. Hariton-Gazal, E., Rosenbluh, J., Graessmann, A., Gilon, C. & Loyter, A. Direct translocation of histone molecules across cell membranes. *J Cell Sci* **116**, 4577-4586 (2003).
83. Sulkowski, P.L. *et al.* Horizontal Transfer of Histone H3 by Mammalian Cells. *bioRxiv*, 2021.2006.2030.450524 (2021).
84. Cohen, M.J., Chirico, W.J. & Lipke, P.N. Through the back door: Unconventional protein secretion. *Cell Surf* **6**, 100045 (2020).
85. Hormazabal, J. *et al.* Chaperone mediated autophagy contributes to the newly synthesized histones H3 and H4 quality control. *Nucleic Acids Research* **50**, 1875-1887 (2022).
86. Ferreira, J.V. *et al.* LAMP2A regulates the loading of proteins into exosomes. *Sci Adv* **8**, eabm1140 (2022).
87. Bernardes, N.E. & Chook, Y.M. Nuclear import of histones. *Biochem Soc Trans* **48**, 2753-2767 (2020).
88. Bowman, G.D. & Poirier, M.G. Post-Translational Modifications of Histones That Influence Nucleosome Dynamics. *Chem Rev* **115**, 2274-2295 (2015).
89. Allfrey, V.G., Faulkner, R. & Mirsky, A.E. ACETYLATION AND METHYLATION OF HISTONES AND THEIR POSSIBLE ROLE IN THE REGULATION OF RNA SYNTHESIS. *Proc Natl Acad Sci U S A* **51**, 786-794 (1964).
90. Morissette, G., Lodge, R., Bouthillier, J. & Marceau, F. Receptor-independent, vacuolar ATPase-mediated cellular uptake of histamine receptor-1 ligands: possible origin of pharmacological distortions and side effects. *Toxicol Appl Pharmacol* **229**, 320-331 (2008).
91. Goldbaum, O. *et al.* Proteasome inhibition stabilizes tau inclusions in oligodendroglial cells that occur after treatment with okadaic acid. *J Neurosci* **23**, 8872-8880 (2003).
92. Forterre, A. *et al.* Proteomic analysis of C2C12 myoblast and myotube exosome-like vesicles: a new paradigm for myoblast-myotube cross talk? *PLoS One* **9**, e84153 (2014).
93. Li, J. *et al.* Serum-free culture alters the quantity and protein composition of neuroblastoma-derived extracellular vesicles. *J Extracell Vesicles* **4**, 26883 (2015).
94. Dar, G.H. *et al.* GAPDH controls extracellular vesicle biogenesis and enhances the therapeutic potential of EV mediated siRNA delivery to the brain. *Nat Commun* **12**, 6666 (2021).
95. Gorgens, A. *et al.* Identification of storage conditions stabilizing extracellular vesicles preparations. *J Extracell Vesicles* **11**, e12238 (2022).
96. Shechter, D., Dormann, H.L., Allis, C.D. & Hake, S.B. Extraction, purification and analysis of histones. *Nat Protoc* **2**, 1445-1457 (2007).
97. Yuan, Z.F. *et al.* EpiProfile 2.0: A Computational Platform for Processing Epi-Proteomics Mass Spectrometry Data. *J Proteome Res* **17**, 2533-2541 (2018).
98. Stenqvist, A.C., Nagaeva, O., Baranov, V. & Mincheva-Nilsson, L. Exosomes secreted by human placenta carry functional Fas ligand and TRAIL molecules and convey apoptosis in activated immune cells, suggesting exosome-mediated immune privilege of the fetus. *J Immunol* **191**, 5515-5523 (2013).
99. Tardoski, S. *et al.* Low-Intensity Ultrasound Promotes Clathrin-Dependent Endocytosis for Drug Penetration into Tumor Cells. *Ultrasound Med Biol* **41**, 2740-2754 (2015).
100. Möbius, W. & Posthuma, G. Sugar and ice: Immunoelectron microscopy using cryosections according to the Tokuyasu method. *Tissue Cell* **57**, 90-102 (2019).

FIGURE LEGENDS

Figure 1. Histones are associated with extracellular vesicles. (A) WB of whole cell lysate (WCL, 10 μg) from a stable OLN-93 cell line expressing human CD63-EGFP and EVs (10, 20 μg) from 100,000 *x*g pellet. CD9, CD63, Tsg101, core histones (H2A, H2B, H3 and H4), Golgi marker GM130 as well as Actb are identified using specific antibodies. Approximate molecular mass is shown in kDa. **(B-E)** Immuno-TEM micrographs of OLN-93 EVs$^{100,000\ xg}$.using primary antibodies as indicated and secondary antibodies conjugated to with 10 nm gold particles. **(B)** Anti-CD63. **(C)** Anti-histone H1 detected using protein A immuno-gold (10 nm) to detect the primary antibody. Scale bar in C = 200 nm. **(D)** Representative immuno-TEM micrographs of OLN-93 cell sections showing anti-CD63 distribution. Insert panel shows a magnified region containing an MVB. The column chart on the right shows quantification of the number of MVBs and ILVs. **T**otal number of MVBs versus CD63$^+$ MVBs, and total number of ILVs versus CD63$^+$ ILVs are shown as % of total. **(E)** OLN-93 sections showing immuno-TEM with anti-H1. Each data point in the column chart shows number of ILVs counted per MVB. Percentages in the column charts refer to % positively labelled ILVs compared to the total (given as 100%). Error bars represent the mean ±SD. **(F)** WB showing localization of a range of membrane, EV and organelle markers together with linker H1 and core histones in OptiPrep purified EVs$^{100,000\ xg}$ (300 μg) fractions from a 12%-36% (w/v) equilibrium density gradient. One 20th of each fraction was loaded on the gel. Experiments were repeated 3 times, and one representative image is shown.

Figure 2. Colocalization of histones and CD63 in ILVs of MVBs. (A-D) Confocal micrographs from a single z-plane of OLN-93 cells showing colocalization of anti-H3 (red) with anti-CD63 (green). Nuclei were counterstained with DAPI (blue). Inset shows a cropped and expanded region of the main image. **(E)** As for A-D but showing Duolink staining (red) due to colocalization of anti-H3 (rabbit) and anti-CD63 (mouse) antibodies. **(F)** Control shows Duolink assay performed in the absence of primary antibodies. **(G)** Immuno-TEM with showing differential labelling of anti-H1 (10 nm gold) and anti-CD63 (5 nm gold). Inset 1 and 2 show high magnification images of the regions indicated in G. Solid arrows indicate anti-H1 labelling, open arrows indicate anti-CD63 labelling. **(H)** Scatter plot showing quantification of CD63 and H1 labelling and colocalization (on the same ILV) in immuno-TEM. A total of 10 images from separate cells and sections were quantified and the numbers of ILVs per MVB are represented by each point. Error bars represent the mean ±SD. **(I)**

Immuno-TEM micrographs of purified OLN-93 EVs showing anti-H1 (5 nm gold) and anti-CD63 (10 nm gold). Full images of these insets are shown in Fig. S4.

Figure 3. **Cellular stress enhances the release of histones. (A)** Schematic diagram outlining the experimental procedure for the heat stress experiment, showing sample collection times. **(B)** WB showing markers (specific antibodies as shown) detected after pulldown of total protein from 1 ml of conditioned media (using StrataClean resin) from Before, Heat stress and After samples., as well as fresh, unconditioned media (Mock). **(C)** WB of $EV^{100,000\ xg}$ fractions (11 µg per lane) isolated from the same conditioned media samples shown in (B). **(D-E)** OLN-93 cells were stressed by heat, LPS, hypoxia, and H_2O_2 followed by WB to quantify histone H2B and H3 in cytoplasmic and EV fractions. Column charts show the ratio between band intensities for stress versus control conditions. Three independent experiments were performed, and one representative WB image is shown. **(F)** Immuno-TEM images of control and stressed OLN-93 cell sections showing ILVs within an MVB. Anti-CD63 detected **(**5 nm gold; **open** arrowheads) and anti-H1 **(**10 nm gold**;** filled arrowheads). **(G)** Analysis showing number of histone positive ILVs present under the various conditions. **(H)** Co-localisation of anti-CD63/H1 in the same ILV under stress conditions. Error bars represent the SD. One-way ANOVA was used to compare control and stress conditions. *, $p < 0.05$, ***, $p < 0.001$. **(I)** Qubit assay showing quantification of ssDNA and dsDNA in OptiPrep fractions from different stress conditions. WBs showing distribution of H3 in each fraction.

Figure 4. Smaller EVs are secreted in response to cellular stress. (A-C) Histograms showing TEM analysis of OLN-93 $EVs^{100,000\ xg}$ from Before, Heat stress and After conditions, comparing size (nm) versus % of total number of EVs counted. Note the presence of two main size distributions: 40-120 nm and 140-200 nm. **(D)** Representative TEM micrographs of negatively stained $EVs^{100,000\ xg}$ isolated from control OLN-93 cells and following exposure to different stress conditions as indicated in each panel. Scale bar = 200 nm. **(E)** Scatter plots showing size distribution of EVs (n = 500) from each condition. Statistical significance (***, $p < 0.001$) using one-way ANOVA followed by Bonferroni's multiple comparison post-test. Horizontal bars in each plot represent the mean diameter in nm, shown below with the ±SD, as well as the mode size (in 10 nm bins).

Figure 5. Histones associate with the EV membrane. (A) Flow diagram showing the procedure used to extract histones from EVs. **(B)** Extraction of histones from OptiPrep purified (fractions 4-7; $EVs^{Optiprep}$) or $EVs^{100,000\ xg}$. Approximately 10 µg EVs were treated with 750 mM NaCl for 24h at 4ºC, followed by ultracentrifugation and analysis of supernatant (s) and pellet (p) fractions by WB. **(C)** Extraction of histones from EVs as described in (B). The pellets from 750 mM NaCl extraction were sonicated and re-pelleted, followed by a second round of extraction with 750 mM NaCl. Fractions (s and p) from each step were compared by WB. **(D)** Extraction of histones from EVs by increasing concentrations of lithium 3,5-diiodosalicylate (10-50 mM) or Triton X-100 (0.1% TX-100). **(E)** TEM images showing control EVs or following 750 mM NaCl or 25 mM lithium 3,5-diiodosalicylate treatment. **(F)** Analysis of histone interaction with liposomes. Histones were mixed with liposomes derived from total lipids of OLN-93 cells and washed in a 100,000 MWCO spin concentrator. The retentate was subjected to WB with anti-histone antibodies. A histone protein-only control (without liposomes) was used to control for lipid-independent retention of histones by the MWCO filter. Recombinant histone proteins (200 ng) were loaded as reference. **(G)** Liposome flotation on a sucrose density gradient (0-40%). Histones were mixed with liposomes and then added to the bottom layer (40% sucrose) of the gradient and subjected to a 15 h ultracentrifugation at 100,000 *x*g. Fractions were analysed by WB. **(H)** Analysis of OLN-93 EVs by WB after trypsin treatment (1:1500-1:150 µg trypsin:µg EV protein). **(I)** Schematic diagram of H2A and H3 cassettes used to express proteins in HEK293 stable cell lines. HA tag is located that the N-terminus and a 6xHis tag at the C-terminus (not to scale). WB analysis of $EVs^{100,000\ xg}$ isolated from stable **(J)** HA-H2A-6xHis or **(K)** HA-H3-6xHis HEK293 cell lines by after trypsin treatment. Location of full-length histones, as well as aggregated (D) or partially degraded (H, J, K) species are indicated by a black or open arrowheads, respectively. Control recombinant histone digestion by trypsin is shown in supplementary Fig. S13.

Figure 6. Histone release via EVs is influenced by multiple pathways. (A) WBs showing the effects of siRNA mediated knock-down of *Alix*, *Tsg101*, and *Smpd2* in OLN-93 cells. H3 and EV markers (Alix, Tsg101 as well as the plasma membrane/microvesicle marker Annexin A1) were quantified in total protein recovered from the media by StrataClean pulldown. The experiment was repeated 4 times, and a representative blot is shown. Band intensities were quantified, and the column chart below shows the ratio of H3

(treated/control) from four independent experiments. **(B)** Pharmacological treatment of OLN-93 cells, analysed as in (A). Control is without treatment. **(C)** Immuno-TEM micrographs showing anti-H1 labelling associated with ILVs in OLN-93 cell sections, following treatment with compounds that significantly increased (3-MA or bafilomycin) or decreased (sodium butyrate) H3 secretion into the media. Right, scatter plot showing quantification of histone positive ILVs under stress conditions. Two-way ANOVA and Bonferroni multiple comparison test was performed: ***, $p < 0.0001$, **, $p < 0.001$, *, < 0.05.

Figure 7: (A) Dot plots showing **r**epresentative IFCM data obtained from HeLa cell conditioned media (CM) and media controls stained with either AF488 labelled anti-H3 or FITC labelled anti-H4 antibodies or stained with a mixture of APC labelled anti-CD9/CD63/CD81 antibodies to detect total tetraspanin positive EVs. **(B)** Quantification of detected gateable events positive for single stained H3, H4, or tetraspanins (n=3) in CM samples collected at different time points from both control and H_2O_2 treated cell cultures. Samples were diluted post staining as indicated on the *y*-axes. **(C)** H3 co-expression and **(D)** H4 co-expression, post double staining with anti-CD9, -CD63, or -CD81 antibodies on CM from 24 h H_2O_2 treated samples. See also Fig. S15. Statistical comparisons by two-way ANOVA. ****, $p < 0.0001$, ***, $p < 0.001$, **, < 0.005. **(E)** Radial plot showing relative abundance of H3 post-translational modifications (PTMs) identified in $EVs^{OptiPrep}$ versus nuclear histones. **(F)** Representative examples of H3 PTMs that are selectively enriched in the nucleus, or in EVs. Lysine (K) trimethylation (Me3) results from the covalent attachment of three Me groups to a K residue and is therefore a relatively “slow” modification. H3 is poorly modified with Me3 in EVs relative to nucleus regardless of whether this PTM benchmarks actively transcribed chromatin (H3K4me3) or silenced heterochromatin (H3K9me3). H3K9 is relatively unmodified in EVs, and H3K79Me2 is an example of a modification that is enriched in EV histones. Phosphorylation of H3S10 is selectively enriched in EVs from LPS treated cells.

Figure 8: Possible pathways for histone secretion via exosomes. Schematic diagram summarizing the findings of this paper. **(A)** Extracellular histones (yellow diamonds) may be internalized by endocytosis and, following endosomal maturation and inward budding into MVBs, would translocate to outer surface of ILVs. Cytoplasmic histones sorted during **(B)** ESCRT-dependent or **(C)** ESCRT–independent (ceramide pathway) ILV formation could

lead to histones as internal/luminal cargo (red diamonds). **(D)** Cytoplasmic histones captured by autophagosomes (green diamonds) may partition to ILVs after autophagosome/amphisome fusion. **(E)** Posttranslational modification of histones in subcellular compartments such as the cytoplasm may also be important for sorting in to MVBs/ILVs. **(F)** The possible trafficking of histones from the nucleus to amphisomes or MVBs is unknown.

SUPPLEMENTARY FIGURE LEGENDS

Supplementary Figure S1. (A) Immuno-TEM images showing anti-tetraspanin CD9 (EV marker) and anti-histone H2A, H2B, H3 and H4 at the surface of OLN-93 EVs$^{100,000\ xg}$. Control (Ctrl) is without primary antibody. Scale bar of 200 nm in H4 applies to all panels. **(B-E)** Immuno-TEM on ultrathin sections of OLN-93 cells showing anti-H2A, H2B, H3 and H4 labelling. Insets show a zoomed region of the main image illustrating staining of ILVs within an MVB. Column charts to the right of each panel show quantification of total number of ILVs per MVB. Percentages in the column charts refer to % positively labelled ILVs compared to the total ILVs. Error bars represent the mean ±SD. Scale bar in E = 100 nm.

Supplementary Figure S2. (A) Line graph showing density of OptiPrep in fractions from a control gradient (without EVs), calculated from A 340 nm measurements (Nanodrop spectrophotometer). **(B)** Representative TEM images of fractions 1 through 12 after separation of OLN-93 EVs$^{100,000\ xg}$. EVs localized predominantly to fractions 3-7. Scale bar in 10 = 200 nm.

Supplementary Figure S3. (Left) WBs of OptiPrep density gradient fractions of EVs$^{100,000\ xg}$ from different cell lines. Different fractions showing the localization of Alix, Tsg101 (Tsg), and histone H3. (Right) Representative TEM images of EVs containing fractions. Scale bars = 0.5 µm/500 nm

Supplementary Figure S4. (A-B) Full images from main figure 2I. images showing Immuno-TEM of OLN-93 EVs (Fraction 3-7, pooled) labelled with anti-histone H1 (5 nm), and anti-CD63 (10 nm) gold particles. Scale bar in A = 100 nm.

Supplementary Figure S5. (A) Immuno-TEM showing sections of Hela cells probed with anti-histone H1 (5 nm), and anti-CD63 (10 nm) gold particles. Inset shows an MVB, which is magnified in the right image. **(B)** Purified EVs (Fraction 3) from the same cells. Inset shows the region of the image, which is shown magnified on the right. Scale bars = 500, 200 or 100 nm as show in each panel.

Supplementary Figure S6. (A) Immuno-TEM showing sections of Caco-2 cells probed with anti-histone H1 (5 nm), and anti-CD63 (10 nm) gold particles. Inset shows an MVB, which is magnified in the right image. **(B)** Purified EVs (Fraction 7) from the same cells. Inset shows the region of the image, which is shown magnified on the right. Scale bars = 500, 200 or 100 nm as show in each panel.

Supplementary Figure S6. (A) Immuno-TEM showing Caco-2 cells sections probed with Anti-histone (5 nm), and Anti-CD63 (10 nm) gold particles. Inset showing MVB. **(B)** Right panel showing EVs purified (Fraction 7) from Caco-2 cells and inset showing part of image.

Supplementary Figure S7. Cell viability assays of OLN-93 under control and stressed conditions. **(A)** Representative images of propidium iodide (PI, stains dead cells) and Hoechst 33343 (also stains live cells) under different conditions. **(B)** Column chart showing percentage of dead cells (% PI/Hoechst; n = 6)- images selected at random. Statistical calculations were performed using Two-way ANOVA and Bonferroni test. **(C-D)** Cell viability assays performed using Annexin V-red (pre-apoptotic/apoptotic cells), and Cytox-green (dead cells). Double stained cells indicate cell death by apoptosis. Cell cultures were labelled and anlaysed using an Incucyte platform (Sartorius, Germany). For panel C, non-parametric T-test was used, for panel D One-way ANOVA and Dunnet`s test was used. *** $p < 0.0005$, ** $p<0.005$.

Supplementary Figure S8. (A) Confocal micrographs (single z-plane) showing immunofluorescence from OLN-93 cells grown under control conditions or following exposure to different stressors. Anti-CD63 (green) and anti-H3 (red). DNA counter stained with DAPI to label the nucleus (blue). Yellow staining indicates areas of colocalization. **(B)** Confocal micrographs of OLN-93 cells additionally subjected to a proximity ligation assay (Duolink; red) between anti-CD63 (mouse; magenta) and anti-H3 (rabbit; green). Red spots indicate proximity labelling between sites of anti-rabbit and anti-

mouse immunoreactivity. **(C-G)** Immuno-TEM of ultrathin sections of OLN-93 cells stained with anti-histone H1 (10 nm gold) and anti-CD63 (5 nm gold). Insets show a higher magnification of an MVB (white boxed region).

Supplementary Figure S9. Confocal micrographs (single z-plane) showing immunofluorescence from OLN-93 cells grown under control conditions, or following exposure to different stressors. Anti-H3 (green) and anti-Annexin A1 (red). DNA counter stained with DAPI to label the nucleus (blue). Inset shows a magnified region of the same z-plane.

Supplementary Figure S10. Quantification of double stranded (dsDNA) and single stranded (ssDNA) in EVs. **(A)** Column charts showing the amount of ds and ss EV associated DNA (ng) per mg of protein, quantified using Qubit assays on OLN-93 EVs in the absence (white bars) or presence (black bars) of Triton X-100 (TX-100). A statistically significant reduction of EV associated DNA was observed between control and 1:150 trypsin:protein ratio (*, $p < 0.05$) using two-way ANOVA followed by Bonferroni's multiple comparison posttest. **(B)** WB of 10 mg of EVs following digestion of DNA with DNase and a 100 KDa filter concentration/washing step. H1 and H3, detected by the anti-histone H3-CT antibody, remain associated with EVs.

Supplementary Figure S11. (A) Line graph showing NTA analysis of OLN-93 $^{EVs100,000\ xg}$ isolated from Before, Heat stress and After samples. A population of smaller particles was most evident in the After sample (blue box). **(B)** Table showing particle data obtained from NTA and BCA (protein concentration) assays. Note, the rate of particle accumulation in the media increases with stress. **(C)** TEM images of EVs$^{100,000\ xg}$. Note the increase in number of smaller particles following stress, which supports the NTA data. **(D)** WB quantification of recombinant H3, used to quantify H3 in media and EVs$^{100,000\ xg}$ samples (Fig. 3B-C). (E) Table summarizing H3 quantification in media versus EVs. Note, H3 increases in the media with stress, even when normalizing for the period of media conditioning. However, the amount of H3 associated with EV remains relatively constant.

Supplementary Figure S12. Quality control of exosomes treated with NaCl or lithium 3,5-diiodosalicylate. **(A)** WB showing extraction of H3 from exosomes when treated with NaCl (250-1000 mM). P = pellet, S: = supernatant. **(B)** Pellets from (A) were examined via

TEM. **(C)** WB showing results of 750 mM NaCl treatment of EVs^{Optiprep} purified EVs obtained following different stress conditions of OLN-93 cells. **(D)** TEM images showing integrity of exosomes after treatment of different lithium 3,5-diiodosalicylate concentrations.

Supplementary Figure S13. WB showing digestion of recombinant histones using trypsin. Approximately 50 ng of each histone was treated with (1:1500-1:150 mg trypsin:mg histone). Samples were separated by SDS-PAGE and detected with the corresponding antibody to investigate pattern of digestion products. The absence of truncated digestion products suggests that free histones do not show preferential site-specific cleavage by trypsin, in contrast to EV associated histones (Fig. 5H, J-K).

Supplementary Figure S14. Effect of drug treatment on OLN-93 cell morphology and viability. **(A)** Phase contrast images showing effect of drug treatment on cell morphology. The indicated concentration of each drug was used to analyze histone secretion in Fig. 6B. **(B)** MTT assay showing cell viability under different drug treatment conditions.

Figure S15: (A) Gating strategy used to identify SSC (low) events. **(B)** Overview of single stained controls used for gating, media controls, and detergent controls (cond. Media +NP40) for experiments using combinations of anti-histone and anti-tetraspanin antibodies, shown in Figure 7C-D.

Supplementary Figure S16. Extraction of histones from OLN-93 cell EVs for analysis of post translational modifications. **(A)** EVs^{Optiprep} (300 µg pooled from fractions 4-7) were used to extract histones by H_2SO_4 acid extraction procedure. Purified protein (1.6 µg) was separated by SDS-PAGE and stained with Comassie R-250. Left panel shows histones extracted from non-treated control EVs. Right panel shows histones extracted with NaCl (750 mM), and after the EV (NaCl) pellet was further extracted with H_2SO_4. **(B)** Similarly, EVs isolated from LPS, and hypoxia conditions were subjected to H_2SO_4 extraction. **(C)** Histones extracted from nuclei of OLN-93 cells. Nuclear histones were used as a reference to compare with EV associated histones.

Supplementary table S1. Table showing concentration of different inhibitors used in previous publications.

Begränsad delning

Supplementary table S2. Excel file containing summary of histone PTM analysis.

AUTHOR CONTRIBUTIONS

Conception: SELA, MH, JG. Design: All authors. Execution: BS, MS, UM, BN, AG, StSt, LS, SiSi, JDG. Writing draft: BS, MS, UM, BN, MH, JDG. Reviewing, and editing: BS, MS, MH, StSt, AG, JZN, OPBW, SiSi, SELA, MH, JDG. All authors read and approved the final manuscript.

Figure 1, Singh *et al.*

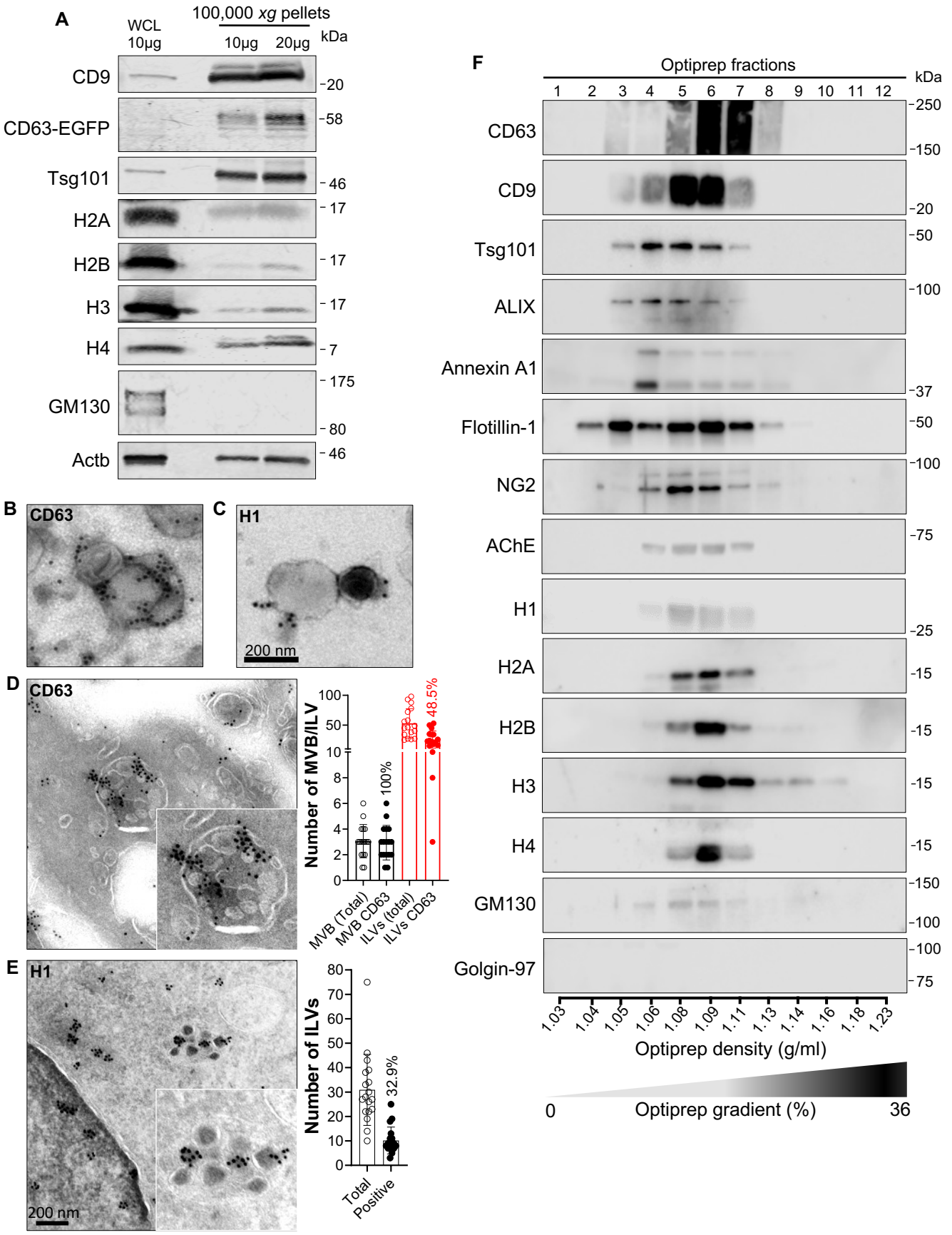

Figure 2, Singh *et al.*

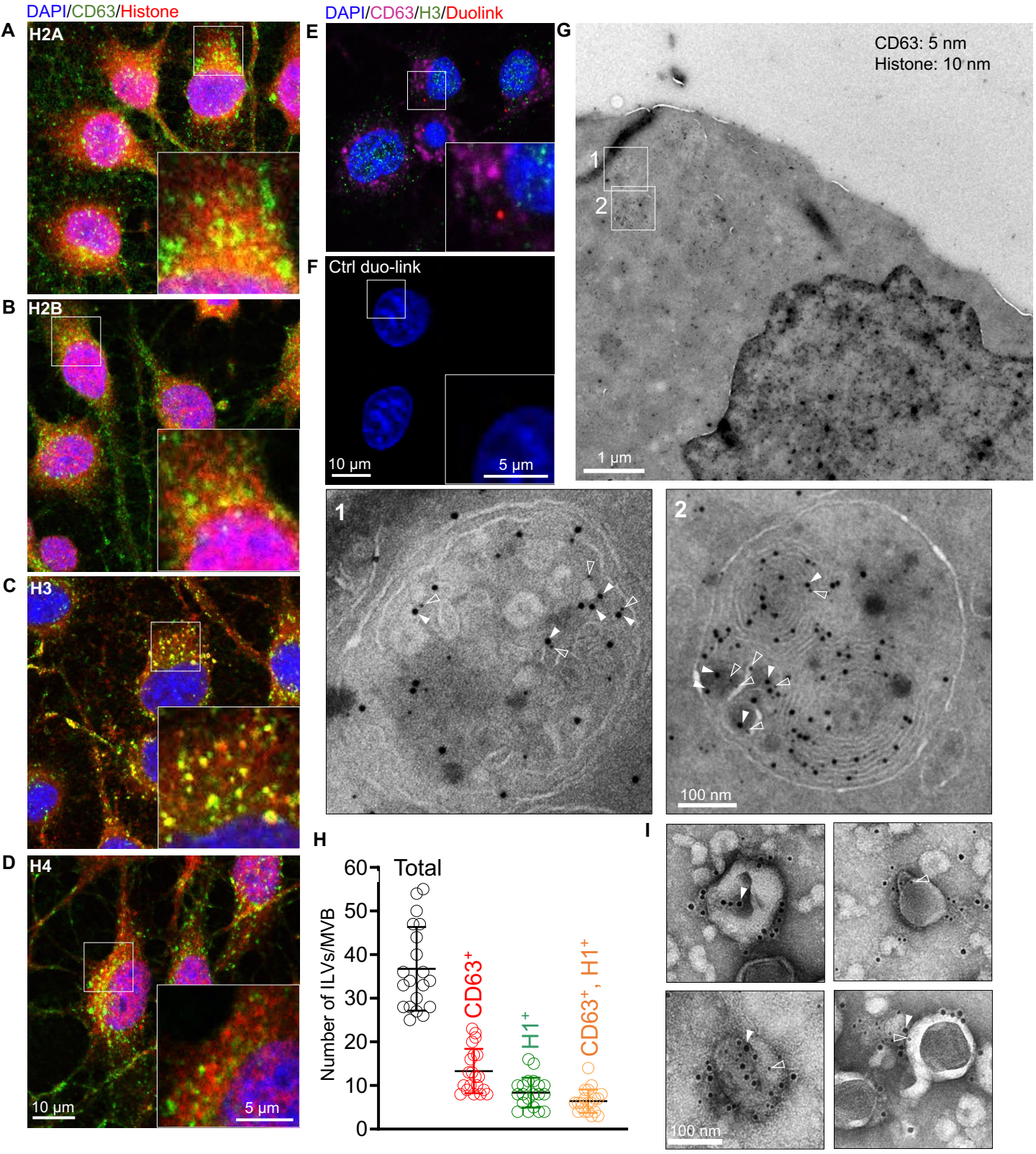

Begränsad delning

Figure 3, Singh *et al.*

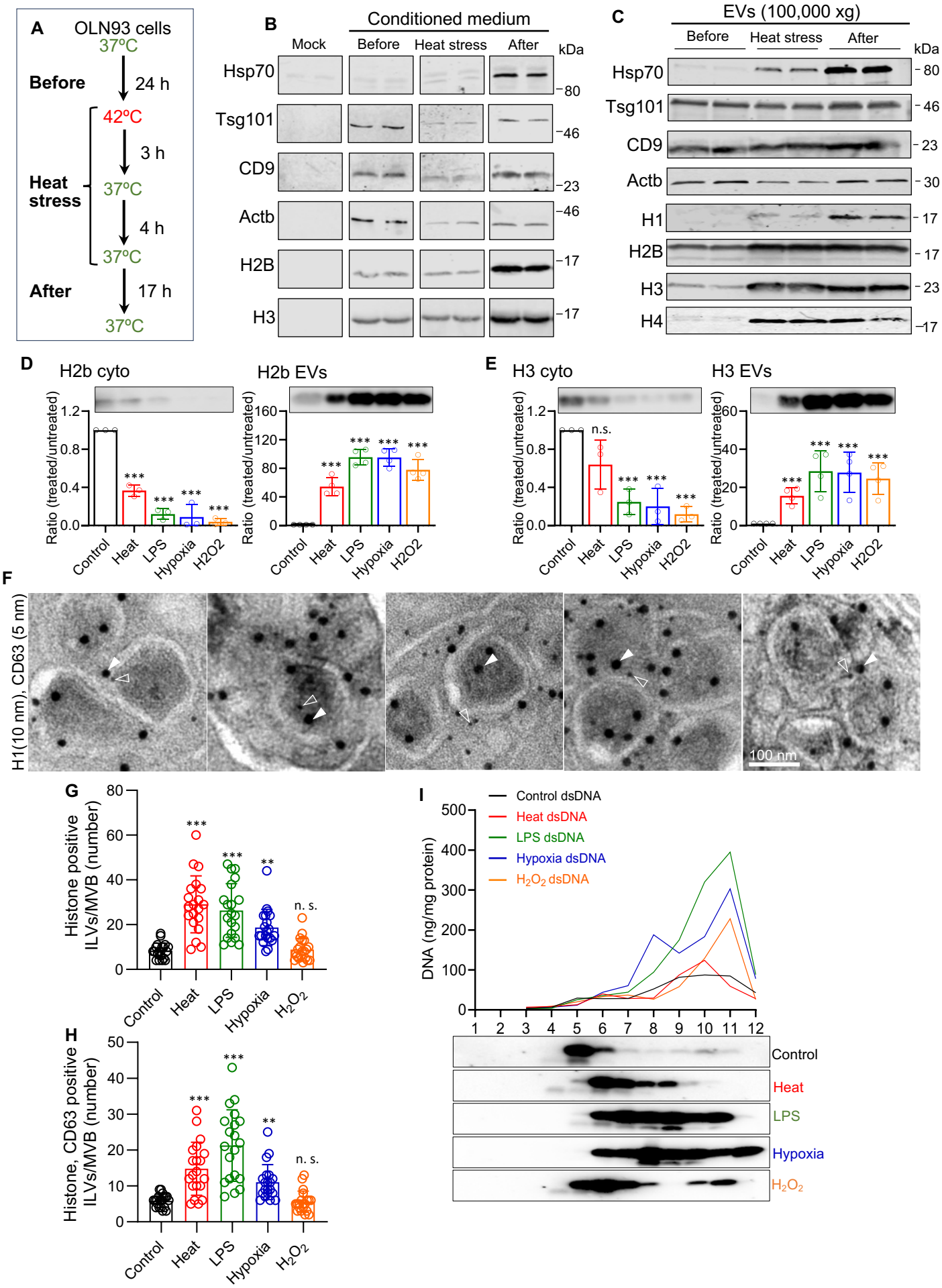

Begränsad delning

Figure 4. Singh *et al.*

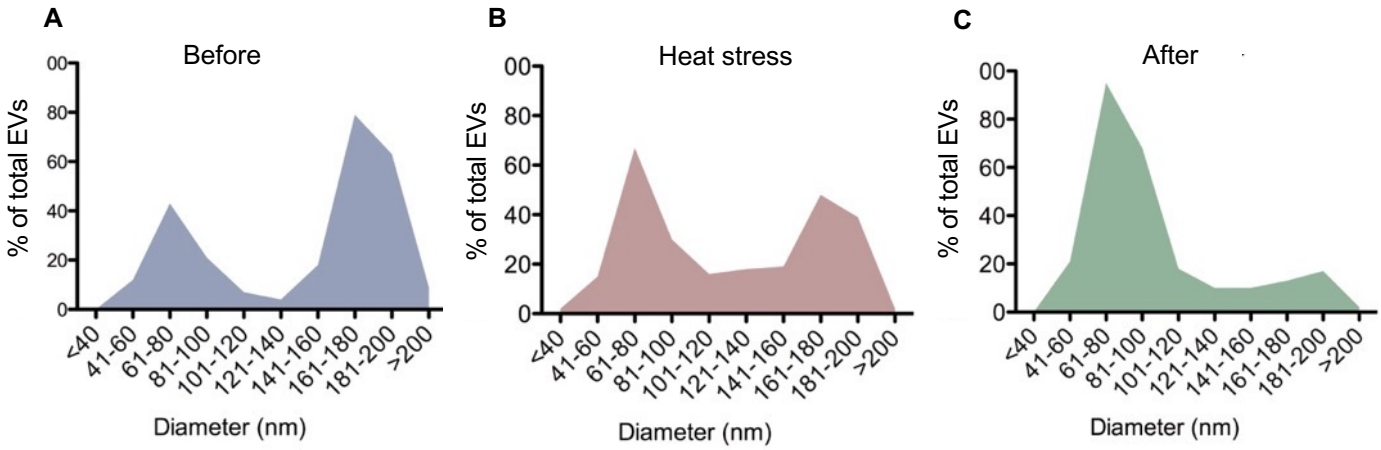

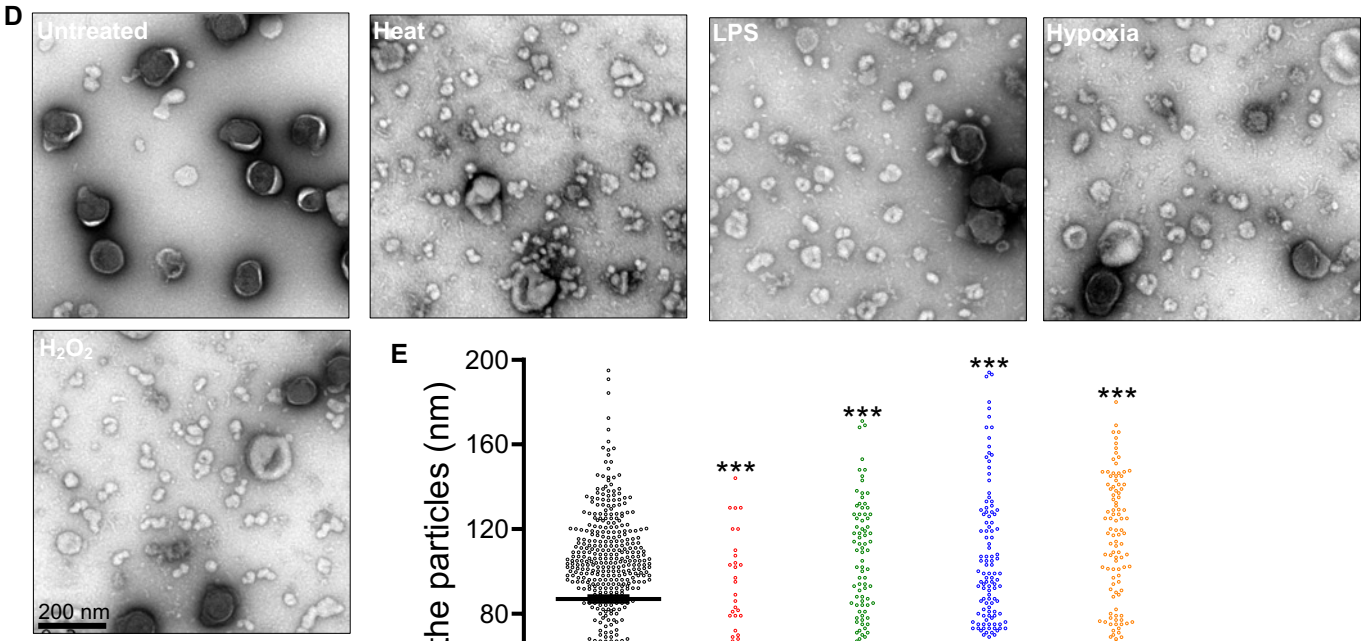

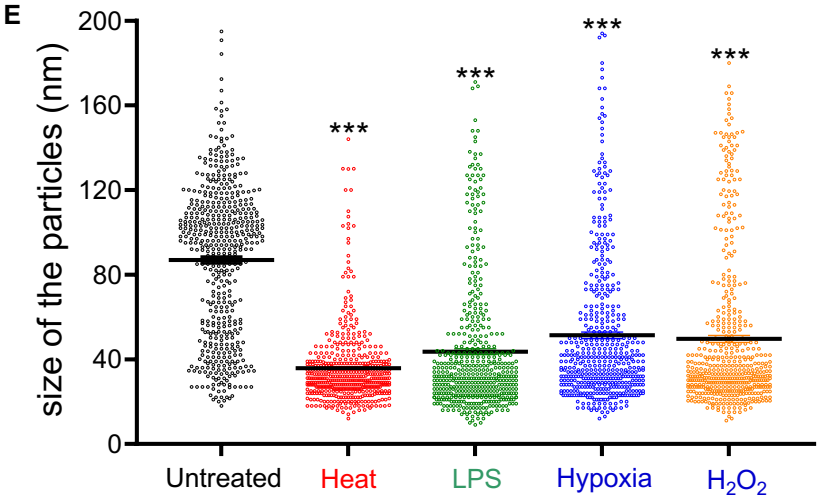

	Untreated	Heat	LPS	Hypoxia	H_2O_2
Mean (nm)	87.0	36.0	43.7	51.6	49.7
SD ±	35.0	18.0	31.7	34.8	36.9
Mode (nm)	100	30	30	30	30

Begränsad delning

Figure 5, Singh *et al.*

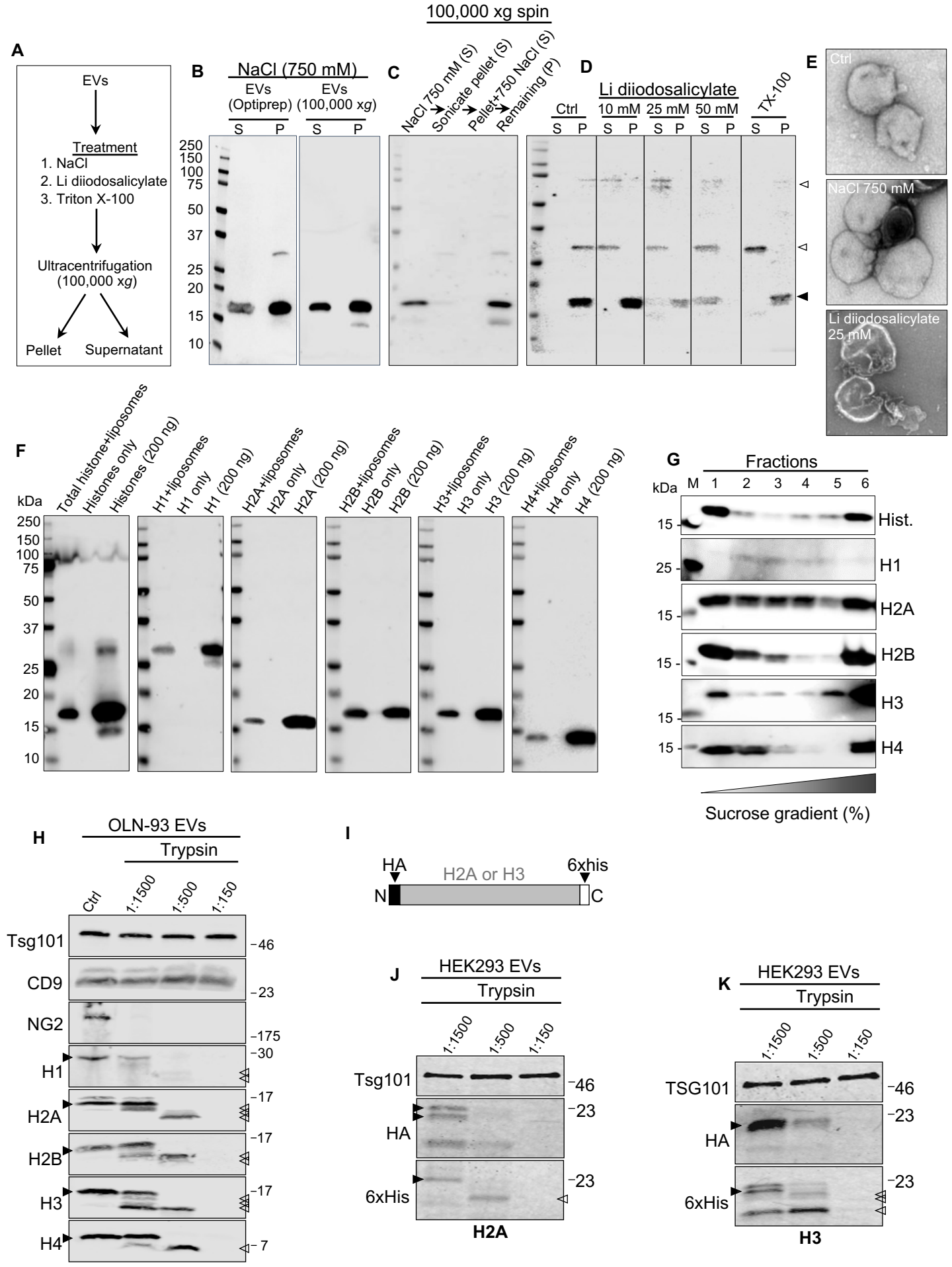

Figure 6, Singh *et al.*

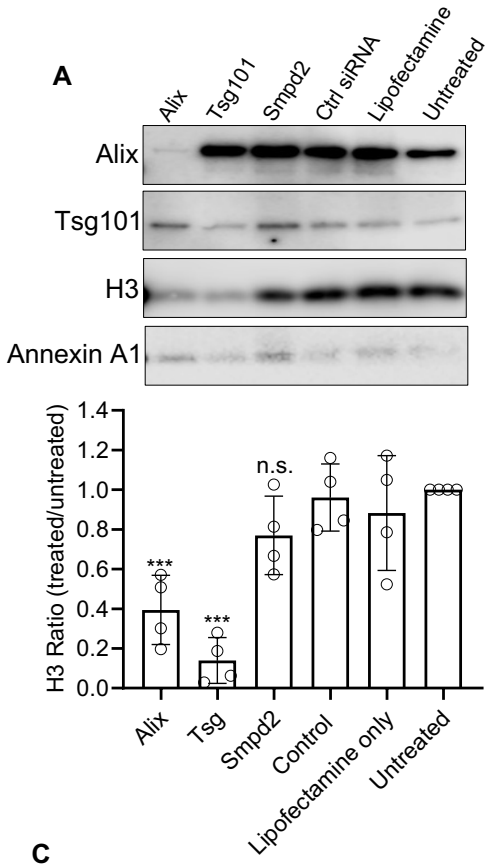

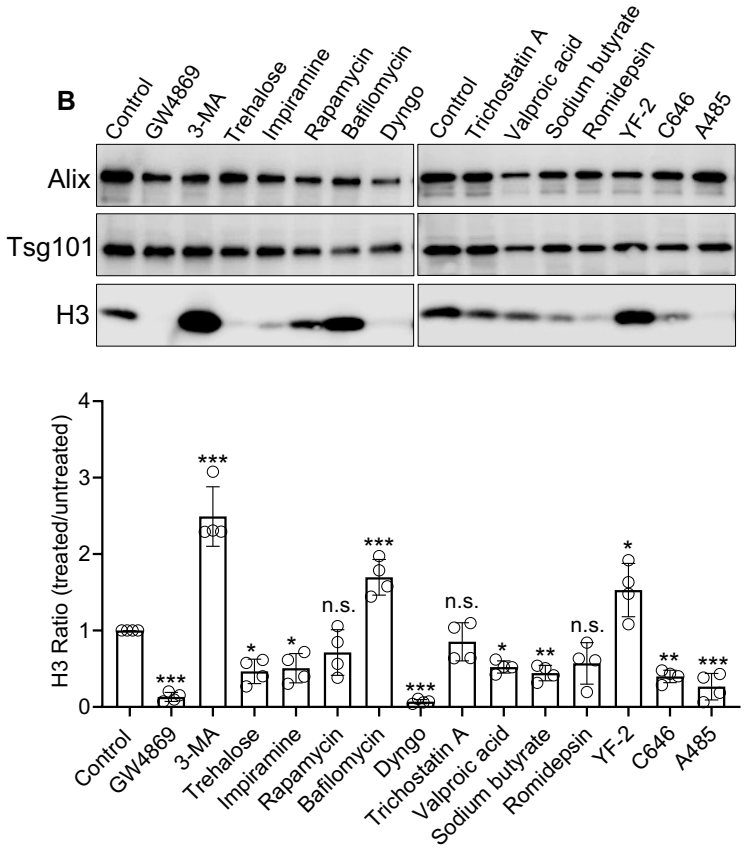

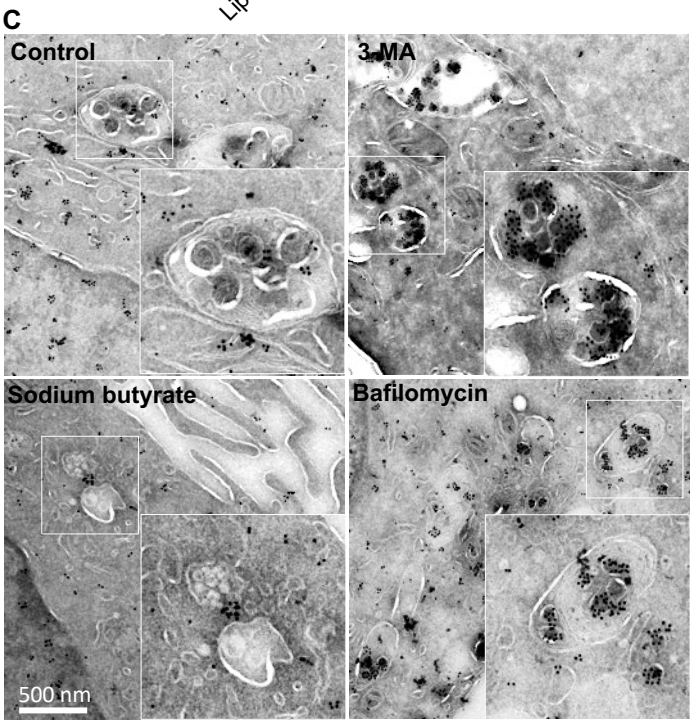

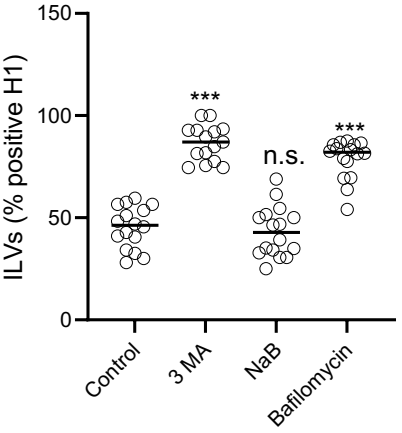

Figure 7, Singh *et al.*

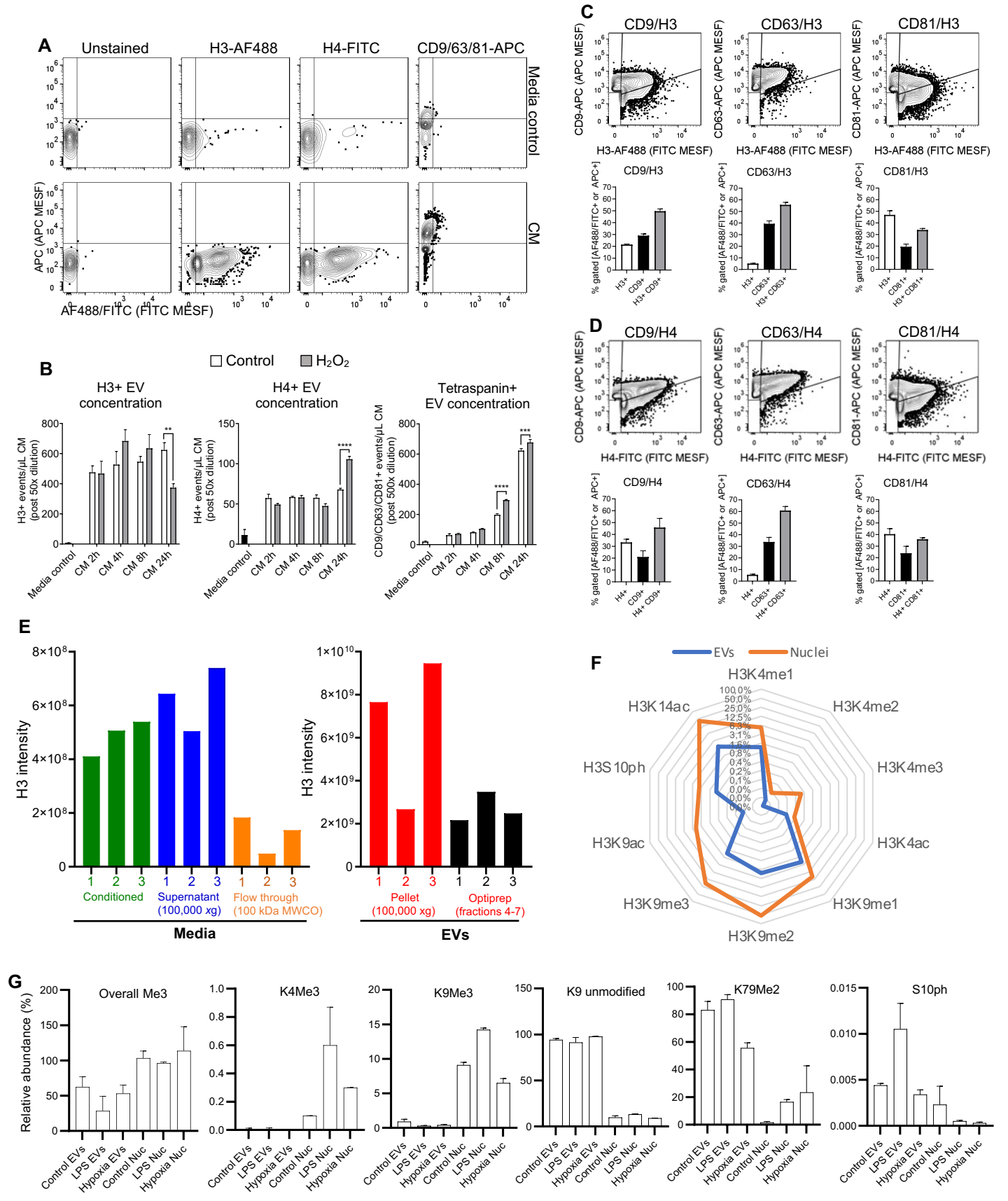
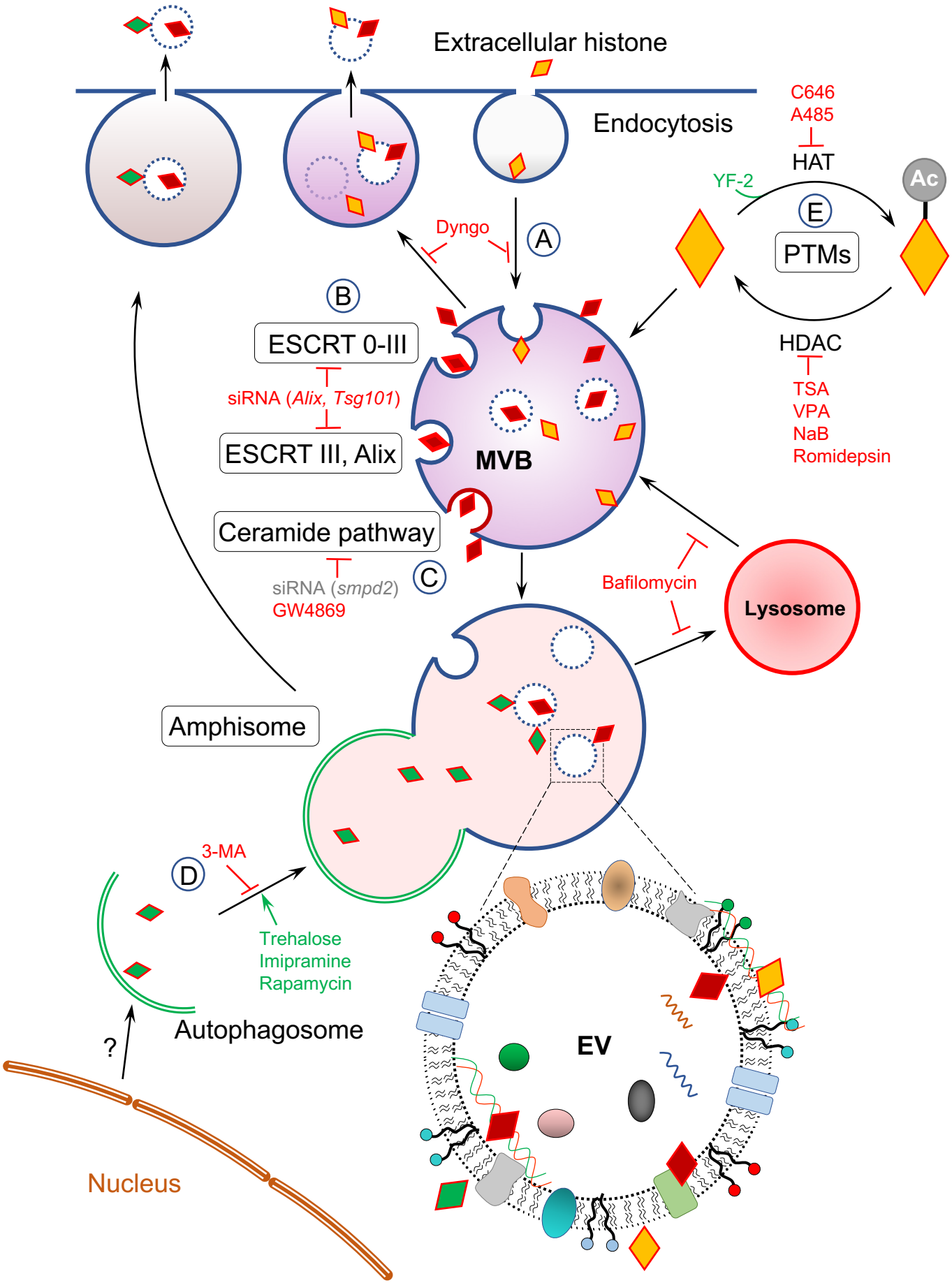
Figure 8, Singh *et al.*